Pharmacological control of angiogenesis by regulating phosphorylation of myosin light chain 2

Kiyomi Tsuji-Tamura*, Mari Sato, and Masato Tamura

[1]Oral Biochemistry and Molecular Biology, Department of Oral Health Science, Faculty of Dental Medicine and Graduate School of Dental Medicine, Hokkaido University, Kita 13, Nishi 7, Kita-Ku, Sapporo 060-8586, Japan

*Author for correspondence: ORCID iD: 0000-0002-0961-5402, Tel or Fax: 011-706-4234, e-mail: ktamuratsuji@den.hokudai.ac.jp

Article types: research articles

Keywords: angiogenesis, myosin light chain 2, MLCP, MLCK, ROCK

Abstract

Background

Control of angiogenesis is widely considered a therapeutic strategy, but reliable control methods are still under development. Phosphorylation of myosin light chain 2 (MLC2), which regulates actin-myosin interaction, is critical to the behavior of vascular endothelial cells (ECs) during angiogenesis. MLC2 is phosphorylated by MLC kinase (MLCK) and dephosphorylated by MLC phosphatase (MLCP) containing a catalytic subunit PP1. We investigated the potential role of MLC2 in the pharmacological control of angiogenesis.

Methods and Results

We exposed transgenic zebrafish *Tg(fli1a:Myr-mCherry)*^{ncv1} embryos to chemical inhibitors and observed vascular development. PP1 inhibition by tautomycetin increased length of intersegmental vessels (ISVs), whereas MLCK inhibition by ML7 decreased it; these effects were not accompanied by structural dysplasia. ROCK inhibition by Y-27632 also decreased vessel length. An *in vitro* angiogenesis model of human umbilical vein endothelial cells (HUVECs) showed that tautomycetin increased vascular cord formation, whereas ML7 and Y-27632 decreased it. These effects appear to be influenced by regulation of cell morphology rather than cell viability or motility. Actin co-localized with phosphorylated MLC2 (pMLC2) was abundant in vascular-like elongated-shaped ECs, but poor in non-elongated ECs. pMLC2 was associated with tightly arranged actin, but not with loosely

arranged actin. Moreover, knockdown of *MYL9* gene encoding MLC2 reduced total MLC2 and pMLC2 protein and inhibited angiogenesis in HUVECs.

Conclusion

The present study found that MLC2 is a pivotal regulator of angiogenesis. MLC2 phosphorylation may be involved in the regulation of of cell morphogenesis and cell elongation. The functionally opposite inhibitors positively or negatively control angiogenesis, probably through the regulating EC morphology. These findings may provide a unique therapeutic target for angiogenesis.

Abbreviations

ANGPT2	angiopoietin 2
DA	dorsal aorta
DLAV	dorsal longitudinal anastomotic vessels
HUVECs	human umbilical vein endothelial cells
ISVs	intersegmental vessels
MLCK	MLC kinase
MLCP	MLC phosphatase
MLC2	myosin light chain 2
MYPT1	myosin phosphatase targeting subunit 1
NO	nitric oxide
NOS	nitric oxide synthase
pMLC2	phosphorylated MLC2
PP1	protein phosphatase 1
ROCK	Rho-associated, coiled-coil containing protein kinase
ECs	vascular endothelial cells
VEGF	vascular endothelial growth factor

1 Introduction

Angiogenesis, the developmental process of a new vascular network from pre-existing vessels in an avascular area, is indispensable for tissue and body growth and is related to both health and disease throughout life. Angiogenesis has been known to aggravate chronic diseases, including diabetes, atherosclerosis, and cancer (for reviews, see [1] [2] [3]). However, in regenerative medicine and tissue engineering, angiogenesis is one of the most pivotal steps in the restoration of blood flow to ischemic tissue and perfusion of grafted tissues (for a review, see [4]). The control of angiogenesis is therefore a challenging issue for therapeutic strategies in angiogenesis-related diseases and regenerative medicine.

The interaction between actin and myosin generates cellular contraction and tension in many types of cells and is responsible for the mechanical properties related to essential cellular processes, including cell motility and morphology [5] (for reviews, see [6][7]). Force generation relies on myosin II, a hexameric protein containing two heavy chains, two essential light chains, and two regulatory light chains (MLC2, also known as MYL9, LC20, RLC). The affinity of myosin for actin is regulated by the phosphorylation of MLC2. MLC2 is phosphorylated by MLC kinase (MLCK) in a calcium/calmodulin-dependent manner and dephosphorylated by MLC phosphatase (MLCP), a trimeric holoenzyme consisting of a protein phosphatase 1 (PP1) catalytic unit, myosin phosphatase targeting subunit 1 (MYPT1) regulatory unit, and a small M20/21 unit (for a review, see [8]). Actin cytoskeleton regulation is also critical for angiogenesis. The MLC2 phosphorylation state has been highly linked to vascular endothelial cell (EC) behavior during angiogenesis. In *in vitro* co-culture angiogenesis models of human umbilical vein endothelial cells (HUVECs) and human dermal fibroblasts, phosphorylated MLC2 (pMLC2) was not detected in HUVECs in the early phase, but was then elevated during the formation of elongated vessel-like structures [9] [10]. The deletion of FOXO1 transcription factor in mice caused embryonic fatality through severe cardiovascular abnormalities, including dilated and enlarged vessels, suggesting the crucial role of FOXO1 in vascular development [11]. The mouse embryonic stem cell (ESC) differentiation system showed that FOXO1-deficient ECs failed to elongate and exhibited abnormal vessel-like structures that were short and thick [11] [12] [13] (for reviews, see [14] [15]). Inhibition of AKT signaling induced cell elongation of ESC-derived ECs in a FOXO1-dependent manner, and this EC elongation was suppressed by the additional inhibition of Rho-associated coiled-coil containing protein kinase (ROCK) by thiazovivin [13]. Recently, we demonstrated that pMLC2 is prominent in normal vessel structures of ESC-derived wild-type ECs, whereas it is lost in aberrant vessels of FOXO1-deficient ECs [16]. FOXO1 possibly suppresses MLCP by transcriptionally upregulating an endogenous PP1 inhibitor PPP1R14C (also known as KEPI), resulting in the accumulation of pMLC2, which in turn elongates ECs and promotes angiogenesis. These studies indicated that the phosphorylation of MLC2 contributes significantly to the establishment of vascular structures.

To examine the potential of MLC2 as a therapeutic target on angiogenesis, this study assessed the effects of MLC2 phosphorylation-related inhibitors on angiogenesis using *in vivo* vascular development of zebrafish embryos and an *in vitro* angiogenesis model of HUVECs, and further investigated the role of MLC2 in angiogenesis using knockdown studies.

2 Materials and methods

2.1 Animals

Animal experiments were conducted with the approval of the Committee on Animal Experimentation of Hokkaido University (No. 21-0078) and followed the institutional guidelines consistent with the Guidelines for Proper Conduct of Animal Experiments (Science Council of Japan, June 1, 2006) and the Law for the Humane Treatment and Management of Animals (Law No. 105, 1973) in Japan. Euthanasia was performed in compliance with the guidelines for the euthanasia of animals of the American Veterinary Medical Association (AVMA, https://www.avma.org/). We attempted to minimize animal suffering and avoid unnecessary trials.

The transgenic zebrafish line Tg(fli1a:Myr-mCherry)^{ncv1} [17] was provided by the National Bioresource Project (NBRP) of Japan. Adult zebrafish were maintained in a 14 h:10 h light/dark cycle at 28°C, and fed with a flake fish food (TetraMin, Tetra, Germany) and brine shrimp (EGGS-90, Kitamura Co., Ltd, Kyoto, Japan) [18]. Fertilized eggs were obtained by bringing a male fish and two female fish together in a breeding tank in the morning on the day of the experiment; the resulting eggs were reared at 28°C in E3 solution (5 mM NaCl, 0.17 mM KCl, 0.33 mM $CaCl_2$, 0.33 mM $MgSO_4$, pH 7.4) supplemented with 0.00001% methylene blue (Cat. No. 133-06962, Wako) and 0.003% N-Phenylthiourea (PTU, a tyrosinase inhibitor, prevents pigmentation) (Cat. No. 27429-22, Nacalai Tesque inc. Kyoto, Japan).

2.2 Cells

Human umbilical vein endothelial cells (HUVECs) (Cat. No. C2519A, Lonza, MD USA) were cultured on plates coated with gelatin (Cat. No. 077-03155, Wako, Tokyo, Japan) in Endothelial Cell Growth Medium Kit (hereinafter referred to as "growth medium", Cat. No. C-22110, Takara Bio Inc., Shiga, Japan). Cells from passages between three and seven were used for studies.

2.3 Inhibitors

Tautomycetin (Cat. No. 2305, Tocris Bioscience, Ellisville, MS, USA), ML7 hydrochloride (ML7) (Cat. No. 4310, R&D System, Inc. Minneapolis, MN, USA), and Y-27632 (Cat. No. HY-10071, MedChemExpress, NJ, USA) were commercially obtained. All inhibitors were dissolved in dimethyl sulfoxide (DMSO) (Cat. No. D4549, Sigma-Aldrich, St. Louis, MO, USA). Control groups were treated with the same amount of DMSO as the maximum dose of the vehicle.

2.4 Inhibitor treatment for zebrafish embryos

Inhibitor treatment was performed as previously described [19] [20]. Fertilized eggs were reared at 10 eggs per well in a 24-well plate filled with E3 solution (with methylene blue and PTU) and exposed to the inhibitors at 6 hours post-fertilization (hpf). Survival was observed at 24 hpf. At 26 and 28 hpf, euthanized embryos were fixed with 4% paraformaldehyde (PFA) in phosphate-buffered saline (PBS)

at 4°C overnight. Fluorescence images of trunk vasculature were acquired using an Axio Imager 2 microscope [Zeiss, Oberkochen, Germany; a dry objective lens (×10, NA 0.3)] and an FV1000D confocal laser scanning microscope [Olympus; a dry objective lens (×10, NA 0.40)]. Unsuitable broken or non-fluorescent embryos were excluded from the analysis. Brightness and contrast adjustments were applied equally for the whole image using ImageJ software version 1.53q [National Institutes of Health (NIH), Bethesda, MD, USA], and no other modifications were made. The lengths of five intersegmental vessels (ISVs) per embryo were measured by manual tracing using ImageJ. The number of ISVs was counted in an anterior part of the middle trunk region.

2.5 Real-time polymerase chain reaction (PCR)

Total RNA from whole zebrafish embryos was isolated using RNAiso Plus (Cat. No. 9108, Takara Bio Inc.) according to the manufacturer's instructions. Reverse transcriptions (RT) were performed from 500 ng of RNA in a 10 mL reaction volume using PrimeScript RT Master Mix (Perfect Real Time) (Cat. No. RP036A, Takara Bio Inc.). Quantitative real-time PCR was performed using Power SYBR Green PCR Master Mix (Cat. No. 4367659, Applied Biosystems, Foster City, CA, USA) for the StepOne real-time PCR system (Applied Biosystems). The primer sequences used for real-time PCR are described below.

2.6 Primers for real-time PCR

The following primers for zebrafish gene expression were used: *angpt2b* fwd 5′-CCAGGGGTTTCAGTGGTACT-3′ and rev 5′-CGCAAGCTTCAAACCACCAT-3′; *vegfaa* fwd 5′-CGACAGAGACACGAAACGTC-3′ and rev 5′-GCTTTGACTTCTGCCTTTGG-3′; *vegfab* fwd 5′-GGTGCTGCAATGATGAAATG-3′ and rev 5′-CACCCTGATGACGAAGAGGT-3′; *nos2b* fwd 5′-GGCTGGCATCTTAAAGCATC-3′ and rev 5′-CAAGAGAGCATGGCGGTATT-3′; *actb1* fwd 5′-CCCTGAATCCCAAAGCCAAC-3′, and rev 5′-ACAGAGAGAGCACAGCCTG-3′. The following primers for human gene expression were used: *MYL9* fwd 5'-AAAGCCAAGACCACCAAGAA-3', and rev 5'-CCATCACGGTTCTGGTCAAT-3'; *ACTB* fwd 5'-AGAGCTACGAGCTGCCTGAC-3', and rev 5'-AGCACTGTGTTGGCGTACAG-3'.

2.7 Three-dimensional (3D) sandwich culture for *in vitro* vascular cord formation and 3D culture for cell morphology analysis

In vitro vascular cord structures were formed in the 3D sandwich culture as previously described [21]. Type I collagen gel (Collagen gel culture kit, Nitta Gelatin, Osaka, Japan) was used for 3D sandwich culture and was prepared according to the instructions. After the bottom layer of the gel had solidified, HUVECs were seeded and cultured in growth medium. Four hours after culture, cells were sandwiched with an upper layer of gel and cultured in growth medium containing 10 ng/ml VEGF-A165 (Cat. No. 450-32, Peprotech, Rocky Hill, NJ, USA) with the test inhibitors for two days. A

green fluorescent calcein-AM (Cat. No. 06735-81, Nacalai Tesque, Kyoto, Japan) was used for live cell staining. Images were obtained using an IX71 fluorescence microscope [Olympus, Tokyo, Japan; a dry objective lens (4×, NA 0.13), (10×, NA 0.30)] or an ECLIPSE TS100 inverted microscope [Nikon Corporation, Tokyo, Japan; a dry objective lens (4×, NA 0.13), (10×, NA0.30)]. Brightness and contrast adjustments were applied equally for the whole image using ImageJ and no other modifications were made. Binary images converted from the original images were used for automated analysis using ImageJ with the Angiogenesis Analyzer plugin tool [22]. "Cords" in the text include all "isolated elements", "branches" and "segments" in the tool. "The average cord length" is the value of "the total length of cords"/"the number of cords" for each field.

To analyze cell morphology, the 3D sandwich culture as described above, with slight modifications, was used. After the bottom layer of the gel had solidified, an upper layer of gel containing HUVECs, at low cell density so that cells exist separately, was overlaid. After the gel solidified, the test inhibitors were added in growth medium containing 10 ng/ml VEGF-A165 for 2 days. Images of live cells stained with calcein-AM were acquired using a fluorescence microscope, and shape descriptors (aspect ratio, circularity, roundness) of each cell were analyzed using the analysis particles tool of ImageJ. The shapes of ECs were classified into three types by aspect ratio, the "round " (1 to less than 1.5) " and "intermediate" (1.5 to less than 2.5) " non-elongated shapes and the "elongated " (2.5 to more) " shape.

2.8 Cell viability assay

HUVECs were seeded on a gelatin-coated plate and cultured in a growth medium. At subconfluent cell density, cells were treated with the indicated doses of inhibitors for two days. The cell viability assay was determined using iMARK Microplate Reader (Bio-Rad Laboratories, Inc. Hercules, CA, USA) with a TetraColor ONE (Seikagaku Corp., Tokyo, Japan). Absorbance was measured at 450 nm and the values for each group were presented as a ratio relative to that of the control.

2.9 Migration assay by scratch-wound method

HUVECs were seeded on a gelatin-coated plate and cultured in a growth medium. At a confluent cell density, the cell monolayer was scratched in a straight line using a 1,000 mL pipette-tip and treated with the indicated doses of the inhibitors. Images of scratched areas were taken using an TS100 microscope (Nikon) immediately after scratching (0 h) and at the endpoint (8 h). The original images were converted to 8-bit gray images, and brightness and contrast adjustments were applied equally for the whole images using ImageJ, and no other modifications were made. Cell-free areas formed by scratching were measured by manually tracing each image. For migration ability, closed areas were determined as the percentage area of each scratch closure by comparing the 0 h and 8 h images.

2.10 Migration assay by transwell insert system

Migration activity was measured using Transwell with 8.0 μm Pore Polyester Membrane Insert (Cat. No. 3464, Corning, NY, USA) in 24-well plates. The insert membrane was coated with gelatin (Cat. No. 077-03155, Wako) and hydrated using Endothelial Cell Basal Medium (hereinafter referred to as "basal medium, Cat. Na. C-22210, Takara) at 37℃ for at least 2 h. Five hundreds μL of growth medium containing 10 ng/ml VEGF-A165, and the inhibitor was placed in each lower chamber. Cells were seeded in 0.2 mL of basal medium at 1.2×10^5 cells per insert (for inhibitor experiments) or 0.3×10^5 cells per insert (for gene knockdown experiments). After 6 h of incubation at 37°C, cells were fixed with 2% PFA, and non-migrated cells on the upper side of the insert membrane were removed with cotton swabs. Nuclear of migrated cells on the lower side of the insert membrane were stained with 4',6-diamidino-2-phenylindole (DAPI, Sigma–Aldrich). Five fields of images from each test were taken using a TS100 microscope (Nikon). The cell number was automatically counted using the analysis particles tool of ImageJ and presented as a percentage of the control.

2.11 Fluorescent staining

HUVECs were maintained in type I collagen gel 3D culture containing VEGF-A165 (10 ng/ml). After 2 days of culture, the 3D gels were dehydrated and flattened using lens paper and filter paper, and fixed in 1.5% PFA in PBS for 15 min at 37 °C, were washed by PBS. Blocking was performed by a blocking buffer containing 0.1% Triton X-100 and 1% skim milk in PBS for overnight at 4 °C. After blocking, the samples were incubation with Phospho-Myosin Light Chain 2 (Ser19) Mouse Monoclonal antibody (mAb) (Cat. No. 3675, Cell Signaling, MA, USA, 1:2000) in a blocking buffer overnight at 4 °C. After washing, the samples were incubated with Goat Anti-Mouse IgG H&L (DyLight 488) preadsorbed (Cat. No. ab96879, Abcam, Cambridge, UK, 1:10000) as a secondary antibody for overnight at 4 °C. Phalloidin-iFluor 555 Reagent (Cat. No. ab176756, Abcam. 1:5000) and DAPI (Sigma–Aldrich) was used for the staining of F-actin and nuclei. Fluorescence images were acquired using the FV1000D confocal laser scanning microscope (Olympus, Tokyo, Japan) and a fluorescence microscope IX71 (Olympus). To observe cell morphology, the original images were adjusted for both contrast and brightness equally using ImageJ. The number of cells with co-localization of pMLC2 with cortical actin or actin stress fibers, as well as cells with tightly or loosely arranged cortical actin, was manually counted on fluorescence images and presented as a percentage of the total cell number.

2.12 The knockdown of gene expression by siRNA

The siRNA knockdown of *MYL9* gene coding for a MLC2 protein was performed in HUVECs. MYL9 siRNA for the target sequence, 5'-TCCAATGTCTTCGCAATGTTTGA-3' was designed by the siRNA online design site siDirect version 2.0 (http://sidirect2.rnai.jp/), and synthesized at Hokkaido System Science Co., Ltd. (Hokkaido, Japan). Silencer Select Negative Control No. 1 siRNA

(4390843, Thermo Fisher Scientific, Inc) was used as a control. The siRNA was transfected into HUVECs using Lipofectamine RNAiMAX (Cat. No. 13778100, Invitrogen, Carlsbad, CA, USA) according to the manufacturer's protocol. After 1-2 days of transfection, the cells were subjected to each experiment.

2.13 Western blotting

Western blotting was performed, as previously reported [21]. An anti-MLC2 rabbit polyclonal antibody (pAb) (Cat. No. 3672, Cell Signaling, 1:200), an anti-phospho-MLC2 (Ser19) mouse mAb (Cat. No. 3675, Cell Signaling, 1:1000) and anti-b-actin rabbit pAb (Cat. No. 20536-1-AP, ProteinTech, 1:2000), and a horseradish peroxidase (HRP)-conjugated donkey anti-rabbit IgG antibody (Cat. No. NA934, Amersham, Buckinghamshire, UK, 1:10000) and HRP-conjugated horse anti-mouse IgG antibody (Cat. No. 7076, Cell Signaling, 1:10000) were diluted by Can Get Signal Immunoreaction Enhancer Solution 1 or 2 (Cat. No. NKB-201, NKB-301, Toyobo, Osaka, Japan), and used as primary or secondary antibodies, respectively.

2.14 Cell count

HUVECs were seeded at the same density and transfected with the siRNA as described above. After 2 days of transfection, the cell number was counted manually using a hemocytometer and presented as a ratio of the control.

2.15 Cell adhesion and spreading assay

Cells detached by trypsin treatment were collected and stained with calcein-AM, and seeded at 0.33×10^4 cells per a well in 0.1 mL of growth medium on 96-Well Cell Imaging Plate with 25 μm film bottom (hereinafter referred to as "film bottom plate", Cat. No. 0030741013, Eppendorf, Hamburg, Germany), which was pre-coated with gelatin for at least 2 hours at 4°C and hydrated by the medium. After incubation for 1 h, plates were gently washed by medium to remove non-adherent cells, and adherent cell images were taken using an TS100 microscope (Nikon). Cell number and size were automatically counted using the analysis particles tool of ImageJ. The size of cells was classified into two types, the "small size" (less than 450 μm^2) " and the "large size" (450 μm^2 to more).

2.16 Statistical analysis

An F-test followed by an unpaired, two-tailed t-test were used as statistical tests for the comparison of two samples. Dunnett's multiple comparison tests were employed to evaluate significant differences between two or more samples using the MEPHAS web tool (http://www.gen-info.osaka-u.ac.jp/testdocs/tomocom/dunnett-e.html). Results are presented as mean ± standard deviation (SD). A P value less than 0.05 was considered statistically significant.

3 Results

3.1 Inhibition of PP1 and MLCK shows contrasting effects on vascular development in zebrafish embryos

Zebrafish embryos are nearly transparent, which facilitates observation of tissue development under stimulation conditions. Therefore, to examine the effects of inhibitors on angiogenesis *in vivo*, we used a transgenic zebrafish strain, *Tg(fli1a:Myr-mCherry)*^{ncv1}, which expresses Myr-mCherry in ECs by the control of the *fli1a* promoter. Embryos were exposed to 0, 10, 50 and 100 nM of tautomycetin, a specific inhibitor of PP1 (Figure 1A–D) and 0, 0.5, 1 and 10 μM of ML7, a selective MLCK inhibitor (Figure 1E-H) from 6 hours post-fertilization (hpf). Zebrafish intersegmental vessels (ISVs) sprout at regular intervals along the dorsal aorta (DA) around 20 hpf, and elongate to the dorsal region, connecting to the dorsal longitudinal anastomotic vessels (DLAV) that are formed by about 36 hpf [23] [24]. In this zebrafish strain, the end of ISVs in the midtrunk region reaches the middle around 26 hpf and the DLAV position around 28 hpf. Therefore, to clarify the effect of the inhibitors, vascular structures were observed in the midtrunk region at 26 hpf for tautomycetin (Figure 1A–D) and 28 hpf for ML7 and Y27632 (Figure 1E-H). Embryos exposed to each inhibitor had a high survival rate at 24 hpf (Figure 1B and F). The number of ISVs was unaffected by these concentrations of each inhibitor (Figure 1C and G). In embryos exposed to 50 and 100 nM, but not 10 nM, of tautomycetin, the length of ISVs increased and reached the DLAV position compared to the partial sprouting ISVs in the 0 nM control group (Figure 1A and D). The length of ISVs in embryos exposed to 0.5, 1 and 10 μM of ML7 was decreased compared to the ISVs that mostly reached the DLAV position in 0 nM control embryos (Figure 1E and H).

ROCK directly phosphorylates MLC2 and further suppresses MLCP activity by phosphorylating MYPT1, thereby increasing pMLC2 [25] (for a review, see [26]). The effects of Y-27632, a ROCK inhibitor, were also examined in angiogenesis *in vivo* (Figure 2). High survival rates were maintained in embryos exposed to 0, 0.5, 1, and 10 μM of Y-27632 (Figure 2B). The number of ISVs remained unaffected by these concentrations of Y-27632 (Figure 2C). In embryos exposed to 1 and 10 μM, but not 0.5 μM, of Y-27632, the length of ISVs was reduced and failed to reach the DLAV position compared to the ISVs in 0 nM control embryos (Figure 2A and D). These results suggest that PP1 inhibition by tautomycetin showed pro-angiogenic effects, whereas MLCK inhibition by ML7 and ROCK inhibition by Y-27632 showed anti-angiogenic effects in vascular development *in vivo*.

Angiogenesis is intricately regulated by diverse factors released by various types of cells, including angiopoietin 2 (ANGPT2), a proangiogenic factor, nitric oxide (NO), an angiogenesis mediator

synthesized by nitric oxide synthase (NOS), and vascular endothelial growth factor (VEGF), a strong proangiogenic factor [27] [28]. The gene expression of these angiogenesis-related factors was elucidated in whole zebrafish embryos exposed to 100 nM of tautomycetin, 10 μM of ML7, and 10 μM of Y-27632 (Figure 2E-H), at effective concentrations for pro- or anti-angiogenesis, respectively (Figures 1 and 2A-D). The expression of zebrafish *angpt2*, *nos2*, *vegfaa,* and *vegfab* genes coding for these angiogenesis-related factors was unaffected by each inhibitor, suggesting that the inhibitors may affect angiogenesis by acting directly on MLC2 phosphorylation in ECs without involving other signaling pathways.

3.2 Inhibition of PP1 and MLCK shows contrasting effects on angiogenesis in human ECs

To determine whether the inhibitor directly affects ECs, we used an angiogenesis model of 3D sandwich collagen gel culture of HUVECs. Cells were treated with tautomycetin and ML7 at a concentration of 0, 3, 5, or 10 nM for 2 days (Figure 3). After calcein-AM staining of live cells, vascular cord structures were observed using a fluorescence microscope. Tautomycetin at 3 and 5 nM increased the number and total length of cords and the average cord length (Figure 3A–D), showing a higher degree of angiogenesis than the 0 nM control. Tautomycetin at 10 nM did not affect angiogenesis and was similar to the control. ML7 at 10 nM suppressed angiogenesis compared to the 0 nM control, and decreased the number and total length of cords and the average cord length, although ML7 at 3 and 5 nM did not affect angiogenesis (Figure 3E–H). Furthermore, we examined the effect of Y-27632 on angiogenesis of HUVECs (Figure 4). Y-27632 at 5 and 10 nM reduced cord number and total length (Figure 4B and C), and the 10 nM treatment reduced the average cord length (Figure 4D). Consistent with the effects *in vivo*, tautomycetin upregulated vascular cord formation in human ECs, while ML7 and Y-27632 downregulated cord formation at certain concentrations. Notably, the change in the average cord length suggests that the inhibitors may affect vessel elongation.

3.3 Inhibition of PP1 and MLCK affects EC elongation, but not cell viability or migration in human ECs

To examine whether the inhibitors affect the angiogenic activity of human ECs, HUVECs were treated with tautomycetin, ML7, and Y-27632 at 3, 5, and 10 nM. All inhibitor-treated HUVECs had a high cell viability, and were not different from the controls (Figure 5A–C). Cell migration activity by scratch-wound assay and transwell insert system was also unaffected by 3 nM of tautomycetin, 10 nM of ML7, and 10 nM of Y-27632 (Figure 5D-G), although each concentration affected vascular cord formation of HUVECs (Figure 3 and 4).

In 3D culture, the morphology of HUVECs changes from non-elongated to elongated in the presence of VEGF. These shifts to elongated shapes were confirmed by analysis of the shape descriptors (Supplementary Table1 control). Treatment with 3 nM of tautomycetin caused a higher aspect ratio,

and lower circularity and roundness than the control (Supplementary Table1). In contrast, treatment with 10 nM of ML7 and 10 nM of Y-27632 decreased aspect ratio, and increased circularity and roundness compared with the control. These results indicate that cells become elongated in the presence of tautomycetin, and more circular in the presence of ML7 and Y-27632. The cell shapes were classified as "round" and "intermediate" non-elongated shapes and "elongated" shape according to the aspect ratio (Figure 5H). In tautomycetin, the percentage of elongated-shaped cells was 38.7%, which was higher than the 13.3% of control cells (Figure 5I). ML7 and Y-27632 suppressed the shift to an elongated shape, lowering them to 2.7% and 3.3%, respectively. Taken together with the inhibitor-induced alteration in the average cord length (Figure 3D and H, and Figure 4D), the inhibitor at a certain concentration may have a significant effect on cell morphology, rather than cell viability or motility.

3.4 EC elongation is accompanied by the interaction between F-actin and pMLC2.

To determine whether EC morphology is related to the interaction between F-actin and pMLC2, fluorescent staining was performed on HUVECs maintained in type I collagen gel 3D cultures containing VEGF-A165 (10 ng/ml) for 2 days (Figure 6 and 7). Round and intermediate-shaped ECs showed strong cortical actin staining, but some cells did not show pMLC2 (Figure 6A and B control). Many of them did not have actin stress fibers with pMLC2. In contrast, many elongated-shaped ECs showed cortical actin and obvious actin stress fibers, which were co-localized with pMLC2. These findings suggest that the interaction between F-actin and pMLC2 may affect EC elongation. This localization of pMLC2 to F-actin was also observed when treated with 3 nM of tautomycetin, 10 nM of ML7, and 10 nM of Y-27632, similar to controls (Figure 6B). When considered together with the effects of inhibitors on EC shapes (Figure 5I), the cell morphological change may be affected by phosphorylation of MLC2, which is modulated by inhibitors.

Furthermore, upon careful observation of the cortical actin arrangement, two distinct patterns were identified: "tightly arranged actin", in which actin filaments form closely packed bundles, and "loosely arranged actin", in which actin filaments are loosely and randomly arranged (Figure 6A and 7A). Tightly arranged actin was co-localized with pMLC2, while many of the loosely arranged actin was not. In the round and intermediate-shaped EC populations, there were cells with tightly arranged actin (60, 36.7%) and cells with loosely arranged actin (40, 63.3%) (Figure 7B control). Elongated-shaped ECs exhibited tightly arranged actin (96.7%) and rarely exhibited loosely arranged actin (3.3%). This relationship between actin arrangement and pMLC2 co-localization was also observed when treated with 3 nM of tautomycetin, 10 nM of ML7, and 10 nM of Y-27632, similar to controls (Figure 7B). The results suggest that a strong correlation exists between pMLC2 and tightly arranged actin filaments, which is particularly noticeable in the elongated morphology.

3.5 Knockdown of MYL9 suppresses angiogenesis in human ECs.

Furthermore, to clarify the role of MLC2 in angiogenesis, we used siRNA-mediated knockdown of the *MYL9* gene, which encodes the MLC2 protein, in HUVECs (Figure 8 and 9A-D). Decreased expression levels of MYL9 mRNA and total MLC2 protein were confirmed in *MYL9*-knockdown HUVECs (Figure 8A-C). The protein levels of pMLC2 were also decreased (Figure 8B and D). In the angiogenesis model of 3D sandwich collagen gel culture, *MYL9*-knockdown reduced the number and total length of cords and the average cord length, namely suppressed angiogenesis (Figure 8E–H), suggesting that MLC2 is required for angiogenesis. *MYL9*-knockdown did not affect cell proliferation by cell number counting (Figure 8I), but decreased cell migration activity in transwell insert system (Figure 8J and K). In morphological analysis in 3D culture, *MYL9*-knockdown decreased aspect ratio, and increased circularity and roundness compared with the control (Supplementary Table2). The proportion analysis of cell shapes showed that *MYL9*-knockdown reduced the percentage of elongated-shaped cells (11.3%), compared to the 46.7% of the control (Figure 8L).

Myosin II in non-muscle tissue has been reported to be involved in cell adhesion (for a review, see [29]). Therefore, cell adhesion and spreading assays were performed. *MYL9*-knockdown did not affect cell adhesion to the gelatin-coated film bottom plate (Figure 9A and B), but reduced the average cell size of adherent cells and the percentage of large sized cells (55.3%) compared to 75.3% of control (Figure 9C and D). These results suggest that MLC2 may promote angiogenesis though the regulation of cell motility and morphology.

4 Discussion

In this study, we found that the regulation of MLC2 phosphorylation may be a promising target for therapeutic angiogenesis. Tautomycetin stimulated vascular development of zebrafish embryos, whereas ML7 and Y-27632 inhibited it. Consistent with the *in vivo* results, the angiogenic effects of tautomycetin and the anti-angiogenic effects of ML7 and Y-27632 were shown in an *in vitro* model of HUVECs. Tautomycetin induced a shift to an elongated shape, whereas ML7 and Y-27632 attenuated the elongation. Co-localization of pMLC2 with actin structures was more pronounced in elongated than in non-elongated ECs. Actin filaments were more tightly arranged when colocalized with pMLC2 than when not colocalized. These results suggest that inhibition of PP1 by tautomycetin may promote EC elongation and angiogenesis by affecting MLC2 phosphorylation, possibly via suppression of MLCP activity. Inhibition of MLCK by ML7 and ROCK signaling by Y-27632 may act directly or indirectly on MLC2 phosphorylation to suppress EC elongation and angiogenesis (Figure 9E). These inhibitors contrastively control angiogenesis by regulating EC morphology. Furthermore, we identified the role of MLC2 in angiogenesis using knockdown studies in HUVECs. *MYL9*-knockdown reduced the levels of total MLC2 and pMLC2, suppressed vascular cord formation, and inhibited

migration, a shift to an elongated shape, and spreading during cell adhesion. The findings revealed that MLC2-mediated regulation of cell motility and morphology is required for angiogenesis.

Tube structures are formed through several mechanisms including cell rearrangement, cell recruitment, cell proliferation, and individual cell elongation without cell proliferation (for a review, see [30]). In angiogenesis, a computational modeling study reported the importance of EC proliferation in vessel growth [31], while *in vivo* analysis showed that EC proliferation is not always necessary for the formation of ISVs and caudal vessels during zebrafish embryogenesis [32]. Our previous report showed that FOXO1-dependent MLC2 phosphorylation positively regulates EC elongation and angiogenesis [16]. In this study, we found the effects of MLC2 phosphorylation-related inhibitors on angiogenesis *in vivo* and *in vitro*. Although EC behavior in angiogenesis is complex, including survival, proliferation, migration, elongation, and motility, and requires careful investigation, these findings indicate that EC elongation via MLC2 phosphorylation may play an important role in angiogenesis.

Several animal studies have shown the effects of inhibitors for PP, MLCK and ROCK signaling on angiogenesis. Oral administration of a PP1 and PP2A inhibitor okadaic acid (17.80 ± 2.41 μg/kg, 24 h) caused structural damage and extensive angiogenesis in the thymus of mice [33]. Treatment with okadaic acid (5–50000 fmol/egg, 3 days) increased extra-embryonic blood vessels on the chick chorioallantoic membrane (CAM) [34]. However, an inhibitor of Akt kinase, MLCK and stromal interaction molecule 1, ML9 (300 μM, 5 days) decreased angiogenesis on CAM induced by fibroblast growth factor-1[35]. Y-27632 (5 mg/kg, 7 days) did not affect basal angiogenesis in mouse retina, but attenuated angiogenesis induced by advanced glycation end products [36]. In the present study, we found that vascular development in zebrafish was increased by tautomycetin (50 and 100 nM, 1 day), and decreased by ML7 (0.5-10 μM, 1 day) and Y-27632 (1 and 10 μM, 1 day). These findings suggest the functionally contrasting inhibitors of MLC2 phosphorylation may positively or negatively control angiogenesis *in vivo*.

PP1 interacts with a wide range of PP1-regulated proteins and is involved in multiple biological process, including the mitogen-activated protein kinase (MAPK) signaling pathway [37], in addition to myosin regulation [38]. MAPK signaling is responsible for the gene expression of angiogenic factors such as VEGF and ANGPT2 [39] [40]. Tautomycetin has been reported to inhibit the activation of RAF1 in MAPK signaling [37]. However, in this study, tautomycetin did not affect gene expressions in zebrafish embryos; this may be explained by intricate signaling networks. Activation of MAPK signaling regulates gene transcription, and its activity is tuned by an extensive number of negative feedback mechanisms [41]. Alternative pathways, such as PI3K-AKT and JAK-STAT

signaling, also regulate VEGF gene expression [42]. Therefore, these complex signaling mechanisms may have influenced the maintenance of gene expression.

The effect of PP inhibitors on EC behaviors has been studied *in vitro*. Okadaic acid increased cell proliferation of human arterial ECs at a concentration of 0.25-1 nM for 48 h [43], and promoted migration in the mouse brain EC line bEnd.3 and human dermal microvascular ECs at a concentration of 100 nM for 24 h [44], and in HUVECs at concentrations of 10–20 nM for 16 h [45]. Vessel-like formation of HUVECs on matrigel was also enhanced at concentrations of 10 and 100 nM for 24 h [45]. Our study showed that PP1 inhibition by tautomycetin (3 and 5 nM, 2 days) promoted vessel-like formation, which correlates with EC morphogenesis, but not cell proliferation and migration. These studies suggest that inhibition of PP may affect EC behavior and thus regulates angiogenesis, but the effects may involve not only MLCP function but also a wide range of other downstream factors of PP1.

In our experiments, tautomycetin showed angiogenic effects *in vivo* zebrafish and *in vitro* HUVEC experiments, but effective concentrations *in vivo* (50 and 100 nM, 20 h) were higher than those *in vitro* (3 and 5 nM, 2 days). The egg envelope (chorion) of zebrafish shields embryos until approximately 72 hpf and has been reported to prevent active uptake of substances [46]. In addition, substances may interact with other cells and molecules in embryos, which may affect inhibitor concentrations at the target cells. Although the exact amount of tautomycetin that passes through the chorion and reaches ECs is unclear, exposure to high concentrations of tautomycetin was required to promote ISV length. However, the possibility remains that the high concentrations *in vivo* may inhibit not only PP1 but also PP2A [47], suggesting that the *in vivo* angiogenic effects of tautomycetin may include both effects of PP1 and PP2A inhibition. Analysis of *in vitro* vascular cord formation showed that tautomycetin induced angiogenesis at 3 and 5 nM for 2 days, but not at 10 nM, and concentration dependent peak response. In mixed lymphocyte reaction assay using splenic lymphocyte, tautomycetin showed the tendency to stimulate lymphocyte proliferation at lower concentrations and peaked at 0.001 μg/ml. After the peak, the proliferation level decreased slowly at 0.01-0.1 μg/ml, and drastically at higher concentrations (1-100 μg/ml) [48]. A dose-dependent biphasic response has been observed in many inhibitor molecules in various biological systems, such as cell proliferation and cell death, and is known as hormesis. A possible mechanism for causing hormesis in inhibitors acting on enzymes involved in dual phosphorylation-dephosphorylation cycles has been proposed using mathematical models [49]. The peak response seen at lower concentrations in our study and others suggests that tautomycetin may have different effects on cell activities depending on the concentration. On the other hand, it has been reported that tautomycetin at a high concentration of 500 nM for 24 h induces a rounded morphology in bEnd.3 [50]. The effects of high concentrations may be due to inhibition of not only PP1 but also PP2A. This is an important issue to be carefully addressed in future research.

The effects of ML7 and Y-27632 on proliferation and migration have been investigated in various cell types. These cell functions were inhibited by ML7 (10 μM) in human aortic smooth muscle cells [51] and by ML7 (20 μM) in human breast cancer cell lines [52]. The effects of Y-27632 are complicated. Proliferation and migration were decreased by Y-27632 (10-40 μM) in human tongue squamous cell carcinoma cell lines [53], but increased by Y-27632 (20 μM) in human periodontal ligament stem cells [54]. Y-27632 (2-200 μM) had no effect on proliferation in mouse renal fibroblasts, and Y-27632 (10-100 μM) inhibited migration in RAW 264.7 mouse macrophages [55]. When ECs were stimulated with VEGF, ML7 (10 μM) and Y-27632 (10 μM) inhibited proliferation and migration in pulmonary arterial ECs [56], HUVECs [57] [58], and human foreskin microvascular ECs [59]. However, there was no effect on the basal level in the absence of other stimuli [56] [60]. In line with these findings, in this study, ML7 and Y-27632 also showed no effects on the proliferation and migration of HUVECs. The effects of inhibitors on EC behaviors may be highly dependent on interactions with other stimuli, and requires further study.

Despite having no effect on cell proliferation and migration, in the present study, low concentrations (10 nM) of ML7 and Y-27632 in the present study inhibited EC elongation and reduced vascular cord formation in 3D culture containing VEGF. Differences in drug responses in diverse culture systems have been reported. The breast cancer cell line JIMT1 was more sensitive to a number of drugs in matrigel 3D culture systems than in 2D cultures [61]. Analysis of gene expression profiling showed a large number of differentially expressed genes between 3D and 2D cultures in JIMT1 cells [61] and primary human fallopian tube secretory epithelial cells [62]. These reports provide insight into the differences in drug sensitivity and cellular response under cell culture conditions, particularly in 2D and 3D environments. Furthermore, in a 2D culture system, ECs are maintained as a flat monolayer on a plastic surface with or without stimulation by growth factors, including VEGF [63], whereas in a 3D culture system ECs can form vascular cord structures in the presence of VEGF. This difference in cell behavior and morphology may have a significant impact on the reactivity to inhibitors. Taken together, these findings suggest that MLC2 phosphorylation-related inhibitors may be able to regulate angiogenesis by directly modulating ECs, although their effects on EC behavior vary depending on experimental conditions.

In this study, a 3D culture assay was required to demonstrate the effects of inhibitors on cell morphology. Therefore, in 3D cultures under the same conditions, we analyzed the relationship between morphological changes and MLC2 phosphorylation. In non-elongated cells, many cells lost pMLC2 in cortical actin and actin stress fibers. In contrast, most elongated cells have prominent pMLC2. These correlations between cell morphology and pMLC2 imply that induction of a shift

toward an elongated shape by tautomycetin would theoretically increase pMLC2, whereas inhibition of the shift by ML7 and Y-27632 would decrease pMLC2.

MLC2 is an essential component to control cytoskeletal dynamics through the interaction between actin and myosin, and regulates not only cell contraction but also various cell functions such as cell proliferation, migration, adhesion, and establishment of cell shape (for a review, see [29]). Knockdown experiments of the *MYL9* gene, which encodes MLC2, showed decreased growth in several cancer cell lines such as human pancreatic ductal adenocarcinoma [64] and human colorectal cancer cells [65]. However, in this study, *MYL9*-knockdown did not affect the proliferation of HUVECs. Cancer cells differ from normal cells in various ways, including uncontrolled rapid growth, lack of contact inhibition, and altered metabolism (for a review, see [66]). Therefore, our results indicate that normal EC proliferation may be independent of MLC2. Migratory activity has been reported to be reduced by *MYL9*-knockdown in a colorectal cancer cell line [65] and human squamous cervical cancer cell lines [67]. Consistent with these reports, *MYL9*-knockdown HUVECs exhibited decreased migratory activity.

Actomyosin networks are recognized as a major regulator in cell adhesion (for a review, see [29]). Several reports have shown that early nascent adhesions form independent of myosin II activity [68] [69]. First, actin filaments apparently assemble at new adhesions, which are subsequently matured and stabilized by the association with myosin II. In this study, cell adhesion and spreading assays revealed that *MYL9*-knockdown had no effect on the adherent cell number of HUVECs and increased adherent cell spreading on the gelatin-coated film surface. These findings appear to be consistent with the known adhesion process. That is, initial adhesion, which is independent of myosin II activity, was unaffected by *MYL9*-knockdown, but subsequent cell spreading, which requires myosin II activity, was inhibited.

MYL9 knockdown in HUVECs inhibited vascular cord formation and suppressed the transition to an elongated shape, similar to the results of treatment with ML7 and Y-27632. *MYL9*-knockdown reduced total MLC2 protein levels, with a concomitant decrease in pMLC2 levels. Therefore, these results indicate the crucial role of MLC2 phosphorylation in altering or maintaining EC morphology. The present study suggests that MLC2 phosphorylation may be essential for endothelial motility and elongated morphogenesis, thereby actively regulating angiogenesis.

How does actin-myosin interaction contribute to EC elongation? The most prominent function of actin-myosin system is cellular contraction, which has largely been demonstrated in studies using muscle cells (myocytes) with abundant the contractile unit sarcomeres. However, actin-myosin system is also involved in a variety of dynamics in non-muscle cells, including cell division, cell movements,

cell adhesion, and even cell shape change (for reviews, see [6] [7] [29] [70]). In cytokinesis in the process of cell division, the contractile ring, a strong assembly of actin filaments and myosin under the cell membrane, gradually squeezes the cytoplasm and pulls the membrane inwards, causing the cell to divide into two (for a review, see [71]). Observations in *Ciona* notochord cells show that an actomyosin ring forms at the front of the cell and then migrates toward the center, contributing to cell elongation [72]. Stress fibers are anchored at their ends to the extracellular matrix at the focal adhesions, so that contractility provides the tension force. When cells are repeatedly stimulated to stretch, the long axis of the cell and the stress fibers are oriented perpendicular to the direction of stretch [73] [74]. Longitudinal orientational order and stability of actin filaments are acquired and enhanced in response to environmental conditions, such as shear stress, cyclic strain and stiff substrates [75] [76] (for a review, see [77]). Cell shape has been reported to interact with stress fibers formation and physical forces [78] [76] [74]. We expect that the above findings from previous research will be applicable to EC morphogenesis in 3D culture. One idea is that the contractile ring-like structure first forms within round-shaped ECs activated by angiogenic stimuli, which gradually compresses the cytoplasm (Supplementary Figure 1). The contractile force by the actin-myosin system in a ring-like state at the center of the cell may cause the cell to deform, perhaps into an elongated shape via a cylindrical shape. Longitudinal stress fibers, which arranged parallel to the long axis of the cell, may then form in response to the physical forces generated by cell deformation in the 3D gel matrix, allowing the elongated cell shape to be maintained. However, many aspects of actomyosin system during cell morphological changes, especially spatio-temporal events, remain unclear, and further research is needed to determine the mechanisms.

When keratinocytes become morphologically polarized, i.e., change from a flat, spread cell shape to a tall, cuboidal cell shape, the localization of pMLC2 increases at the cell periphery, and the array of loose actin filaments gradually narrows [68]. Myosin function is essential for the formation of the cuboidal morphology, as inhibition of myosin II ATPase activity by blebbistatin reduces lateral domain height during polarization [68]. In this report, we observed EC morphology in a 3D angiogenesis model. Non-elongated ECs showed loosely aligned cortical actin, few actin stress fibers and poor pMLC2 localization, whereas elongated ECs showed tightly arranged cortical actin bundles, strong actin stress fibers and clear localization of pMLC2. These studies in non-muscle cell morphogenesis suggest that pMLC2 may play a role in bundling and stabilizing loose pre-existing actin filaments present in each part of the cells (A schematic model in Figure 7A).

Signaling molecules with potent effects on angiogenesis, such as VEGF, are the main targets for both pro- and anti-angiogenic therapies [79] (for a review, see [3]). However, the limitations of the effectiveness and negative issues have also been shown (for reviews, see [4] [80]). Experimental alterations of VEGF signaling in zebrafish have been reported to cause severe morphological

abnormalities in vascular structure; overexpression of *vegf* induced ectopic vessels [81], and the knockdown caused vessel loss [82]. Our *in vivo* studies demonstrated the possibility of pharmacologically controlling angiogenesis by positively or negatively regulating MLC2 phosphorylation. Notably, the effects were not associated with vascular dysplasia and retained intact vascular structures. Moreover, our *in vitro* study revealed the direct cell effects of inhibitors and the role of MLC2 on EC morphology. MLC2 phosphorylation may be useful as a unique target for therapeutic angiogenesis.

Ethical approval

This study was approved by the Committee on Animal Experimentation of Hokkaido University (No. 21-0078).

Funding

This work was supported by the Japan Society for the Promotion of Science (JSPS; grant numbers KAKENHI 22K10186).

Author contributions

Kiyomi Tsuji-Tamura developed the research plans and performed the experiments and analyses. Mari Sato and Masato Tamura contributed to the fish maintenance and experiments. The first draft of the manuscript was written by Kiyomi Tsuji-Tamura and all authors commented on previous versions of the manuscript. All authors read and approved the final manuscript.

Declaration of competing interest

The authors have no relevant financial or non-financial interests to disclose.

Acknowledgment

Not applicable.

Data availability

The datasets obtained during this study are available from the corresponding author upon reasonable request.

References

[1] R. Cheng, J. xing Ma, Angiogenesis in diabetes and obesity, Rev Endocr Metab Disord 16 (2015) 67–75. https://doi.org/10.1007/s11154-015-9310-7.

[2] K. Theodorou, R.A. Boon, Endothelial cell metabolism in atherosclerosis, Front Cell Dev Biol 6 (2018). https://doi.org/10.3389/fcell.2018.00082.

[3] A.S. Oguntade, F. Al-Amodi, A. Alrumayh, M. Alobaida, M. Bwalya, Anti-angiogenesis in cancer therapeutics: the magic bullet, J Egypt Natl Canc Inst 33 (2021). https://doi.org/10.1186/s43046-021-00072-6.

[4] M.M. Martino, S. Brkic, E. Bovo, M. Burger, D.J. Schaefer, T. Wolff, L. Gürke, P.S. Briquez, H.M. Larsson, R. Gianni-Barrera, J.A. Hubbell, A. Banfi, Extracellular matrix and growth factor engineering for controlled angiogenesis in regenerative medicine, Front Bioeng Biotechnol 3 (2015). https://doi.org/10.3389/fbioe.2015.00045.

[5] K. Tsuji-Tamura, M. Ogawa, Dual inhibition of mTORC1 and mTORC2 perturbs cytoskeletal organization and impairs endothelial cell elongation, Biochem Biophys Res Commun 497 (2018) 326–331. https://doi.org/10.1016/j.bbrc.2018.02.080.

[6] R. Levayer, T. Lecuit, Biomechanical regulation of contractility: Spatial control and dynamics, Trends Cell Biol 22 (2012) 61–81. https://doi.org/10.1016/j.tcb.2011.10.001.

[7] M. Vicente-Manzanares, X. Ma, R.S. Adelstein, A.R. Horwitz, Non-muscle myosin II takes centre stage in cell adhesion and migration, Nat Rev Mol Cell Biol 10 (2009) 778–790. https://doi.org/10.1038/nrm2786.

[8] M. Eto, T. Kitazawa, Diversity and plasticity in signaling pathways that regulate smooth muscle responsiveness: Paradigms and paradoxes for the myosin phosphatase, the master regulator of smooth muscle contraction, Journal of Smooth Muscle Research 53 (2017) 1–19. https://doi.org/10.1540/jsmr.53.1.

[9] G. Mavria, Y. Vercoulen, M. Yeo, H. Paterson, M. Karasarides, R. Marais, D. Bird, C.J. Marshall, ERK-MAPK signaling opposes Rho-kinase to promote endothelial cell survival and sprouting during angiogenesis, Cancer Cell 9 (2006) 33–44. https://doi.org/10.1016/j.ccr.2005.12.021.

[10] S. Abraham, M. Yeo, M. Montero-Balaguer, H. Paterson, E. Dejana, C.J. Marshall, G. Mavria, VE-Cadherin-Mediated Cell-Cell Interaction Suppresses Sprouting via Signaling to MLC2 Phosphorylation, Current Biology 19 (2009) 668–674. https://doi.org/10.1016/j.cub.2009.02.057.

[11] T. Furuyama, K. Kitayama, Y. Shimoda, M. Ogawa, K. Sone, K. Yoshida-Araki, H. Hisatsune, S.I. Nishikawa, K. Nakayama, K. Nakayama, K. Ikeda, N. Motoyama, N. Mori, Abnormal angiogenesis in Foxo1 (Fkhr)-deficient mice, Journal of Biological Chemistry 279 (2004) 34741–34749. https://doi.org/10.1074/jbc.M314214200.

[12] S.-H. Park, H. Sakamoto, K. Tsuji-Tamura, T. Furuyama, M. Ogawa, Foxo1 is essential for in vitro vascular formation from embryonic stem cells, Biochem Biophys Res Commun 390 (2009). https://doi.org/10.1016/j.bbrc.2009.10.063.

[13] K. Tsuji-Tamura, M. Ogawa, Inhibition of the PI3K-Akt and mTORC1 signaling pathways promotes the elongation of vascular endothelial cells, J Cell Sci 129 (2016) 1165–1178. https://doi.org/10.1242/jcs.178434.

[14] K. Tsuji-Tamura, H. Sakamoto, M. Ogawa, ES Cell Differentiation as a Model to Study Cell Biological Regulation of Vascular Development, in: Embryonic Stem Cells: The Hormonal Regulation of Pluripotency and Embryogenesis (Ed. C. S. Atwood), 2011: pp. 581–606. https://doi.org/10.5772/14101.

[15] K. Tsuji-Tamura, M. Ogawa, Morphology regulation in vascular endothelial cells, Inflamm Regen 38 (2018). https://doi.org/10.1186/s41232-018-0083-8.

[16] K. Tsuji-Tamura, M. Ogawa, FOXO1 promotes endothelial cell elongation and angiogenesis by up-regulating the phosphorylation of myosin light chain 2, Angiogenesis (2023). https://doi.org/10.1007/s10456-023-09884-7.

[17] S. Fukuhara, J. Zhang, S. Yuge, K. Ando, Y. Wakayama, A. Sakaue-Sawano, A. Miyawaki, N. Mochizuki, Visualizing the cell-cycle progression of endothelial cells in zebrafish, Dev Biol 393 (2014) 10–23. https://doi.org/10.1016/j.ydbio.2014.06.015.

[18] Graham J. Lieschke, Andrew C. Oates, Koichi Kawakami, eds., Zebrafish: Methods and Protocols, Humana Press, n.d. www.springer.com/series/7651 (accessed February 15, 2023).

[19] K. Tsuji-Tamura, M. Sato, M. Fujita, M. Tamura, Glycine exerts dose-dependent biphasic effects on vascular development of zebrafish embryos, Biochem Biophys Res Commun 527 (2020) 539–544. https://doi.org/10.1016/j.bbrc.2020.04.098.

[20] K. Tsuji-Tamura, M. Sato, M. Fujita, M. Tamura, The role of PI3K/Akt/mTOR signaling in dose-dependent biphasic effects of glycine on vascular development, Biochem Biophys Res Commun 529 (2020) 596–602. https://doi.org/10.1016/j.bbrc.2020.06.085.

[21] K. Tsuji-Tamura, S. Morino-Koga, S. Suzuki, M. Ogawa, The canonical smooth muscle cell marker TAGLN is present in endothelial cells and is involved in angiogenesis, J Cell Sci 134 (2021). https://doi.org/10.1242/jcs.254920.

[22] G. Carpentier, S. Berndt, S. Ferratge, W. Rasband, M. Cuendet, G. Uzan, P. Albanese, Angiogenesis Analyzer for ImageJ — A comparative morphometric analysis of "Endothelial Tube Formation Assay" and "Fibrin Bead Assay," Sci Rep 10 (2020). https://doi.org/10.1038/s41598-020-67289-8.

[23] S. Isogai, M. Horiguchi, B.M. Weinstein, The vascular anatomy of the developing zebrafish: An atlas of embryonic and early larval development, Dev Biol 230 (2001) 278–301. https://doi.org/10.1006/dbio.2000.9995.

[24] S. Isogai, N.D. Lawson, S. Torrealday, M. Horiguchi, B.M. Weinstein, Angiogenic network formation in the developing vertebrate trunk, Development 130 (2003) 5281–5290. https://doi.org/10.1242/dev.00733.

[25] G. Totsukawa, Y. Yamakita, S. Yamashiro, D.J. Hartshorne, Y. Sasaki, F. Matsumura, Distinct Roles of ROCK (Rho-kinase) and MLCK in Spatial Regulation of MLC Phosphorylation for Assembly of Stress Fibers and Focal Adhesions in 3T3 Fibroblasts, J Cell Biol 150 (2000) 797–806. http://www.jcb.org.

[26] K. Riento, A.J. Ridley, ROCKs: multifunctional kinases in cell behaviour, Nat Rev Mol Cell Biol 4 (2003) 446–456. https://doi.org/10.1038/nrm1128.

[27] I.B. Lobov, P.C. Brooks, R.A. Lang, Angiopoietin-2 displays VEGF-dependent modulation of capillary structure and endothelial cell survival in vivo, (n.d.). https://www.pnas.org.

[28] D. Fukumura, T. Gohongi, A. Kadambi, Y. Izumi, J. Ang, C.-O. Yun, D.G. Buerk, P.L. Huang, R.K. Jain, Predominant role of endothelial nitric oxide synthase in vascular endothelial growth factor-induced angiogenesis and vascular permeability, Proc Natl Acad Sci U S A. 98 (2001) 2604–2609. https://doi.org/10.1073/pnas.041359198.

[29] S. Tojkander, G. Gateva, P. Lappalainen, Actin stress fibers - Assembly, dynamics and biological roles, J Cell Sci 125 (2012) 1855–1864. https://doi.org/10.1242/jcs.098087.

[30] D.J. Andrew, A.J. Ewald, Morphogenesis of epithelial tubes: Insights into tube formation, elongation, and elaboration, Dev Biol 341 (2010) 34–55. https://doi.org/10.1016/j.ydbio.2009.09.024.

[31] K.A. Norton, A.S. Popel, Effects of endothelial cell proliferation and migration rates in a computational model of sprouting angiogenesis, Sci Rep 6 (2016). https://doi.org/10.1038/srep36992.

[32] S. Fukuhara, J. Zhang, S. Yuge, K. Ando, Y. Wakayama, A. Sakaue-Sawano, A. Miyawaki, N. Mochizuki, Visualizing the cell-cycle progression of endothelial cells in zebrafish, Dev Biol 393 (2014) 10–23. https://doi.org/10.1016/j.ydbio.2014.06.015.

[33] E. Ottaviani, A. Franchini, E. Marchesini, R. Poletti, E. Ottaviani, Swiss mice CD1 fed on mussels contaminated by okadaic acid and yessotoxins: effects on thymus and spleen, 2004.

[34] Oikawa T, Suganuma M, Ashino-Fuse H, Shimamura M, Okadaic acid is a potent angiogenesis inducer, Jpn J Cancer Res 83 (1992) 6–9. https://doi.org/10.1111/j.1349-7006.1992.tb02343.x.

[35] R. Forough, B. Weylie, C. Patel, S. Ambrus, U.S. Singh, J. Zhu, Role of AKT/PKB signaling in fibroblast growth factor-1 (FGF-1)-induced angiogenesis in the chicken chorioallantoic membrane (CAM), J Cell Biochem 94 (2005) 109–116. https://doi.org/10.1002/jcb.20274.

[36] L. Chen, Y. Cui, B. Li, J. Weng, W. Wang, S. Zhang, X. Huang, X. Guo, Q. Huang, Advanced glycation end products induce immature angiogenesis in in vivo and ex vivo mouse models, Am J Physiol Heart Circ Physiol 318 (2020) 519–533. https://doi.org/10.1152/ajpheart.00473.2019.-Proliferative.

[37] S. Mitsuhashi, H. Shima, N. Tanuma, N. Matsuura, M. Takekawa, T. Urano, T. Kataoka, M. Ubukata, K. Kikuchi, Usage of tautomycetin, a novel inhibitor of protein phosphatase 1 (PP1),

reveals that PP1 is a positive regulator of Raf-1 in vivo, Journal of Biological Chemistry 278 (2003) 82–88. https://doi.org/10.1074/jbc.M208888200.

[38] D. ALESSI, L.K. MACDOUGALL, M.M. SOLA, M. IKEBE, P. COHEN, The control of protein phosphatase-1 by targetting subunits: The major myosin phosphatase in avian smooth muscle is a novel form of protein phosphatase-1, Eur J Biochem 210 (1992) 1023–1035. https://doi.org/10.1111/j.1432-1033.1992.tb17508.x.

[39] G. Schäfer, T. Cramer, G. Suske, W. Kemmner, B. Wiedenmann, M. Höcker, Oxidative stress regulates vascular endothelial growth factor-A gene transcription through Sp1- and Sp3-dependent activation of two proximal GC-rich promoter elements, Journal of Biological Chemistry 278 (2003) 8190–8198. https://doi.org/10.1074/jbc.M211999200.

[40] A. Hegen, S. Koidl, K. Weindel, D. Marmé, H.G. Augustin, U. Fiedler, Expression of angiopoietin-2 in endothelial cells is controlled by positive and negative regulatory promoter elements, Arterioscler Thromb Vasc Biol 24 (2004) 1803–1809. https://doi.org/10.1161/01.ATV.0000140819.81839.0e.

[41] D. Lake, S.A.L. Corrêa, J. Müller, Negative feedback regulation of the ERK1/2 MAPK pathway, Cellular and Molecular Life Sciences 73 (2016) 4397–4413. https://doi.org/10.1007/s00018-016-2297-8.

[42] A. Matsumura, T. Kubota, H. Taiyoh, H. Fujiwara, K. Okamoto, D. Ichikawa, A. Shiozaki, S. Komatsu, M. Nakanishi, Y. Kuriu, Y. Murayama, H. Ikoma, T. Ochiai, Y. Kokuba, T. Nakamura, K. Matsumoto, E. Otsuji, HGF regulates VEGF expression via the c-Met receptor downstream pathways, PI3K/Akt, MAPK and STAT3, in CT26 murine cells, Int J Oncol 42 (2013) 535–542. https://doi.org/10.3892/ijo.2012.1728.

[43] I. Spyridopoulos, P. Mayer, K.S. Shook, D.I. Axel, R. Viebahn, K.R. Karsch, Loss of cyclin A and G1-cell cycle arrest are a prerequisite of ceramide-induced toxicity in human arterial endothelial cells, Cardiovasc Res 50 (2001) 97–107. www.elsevier.com/locate/cardioreswww.elsevier.nl/locate/cardiores.

[44] M.R.I. Young, K. Kolesiak, J. Meisinger, Protein phosphatase-2A regulates endothelial cell motility and both the phosphorylation and the stability of focal adhesion complexes, Int J Cancer 100 (2002) 276–282. https://doi.org/10.1002/ijc.10491.

[45] Y.S. Kim, K.H. Ahn, S.Y. Kim, J.W. Jeong, Okadaic acid promotes angiogenesis via activation of hypoxia-inducible factor-1, Cancer Lett 276 (2009) 102–108. https://doi.org/10.1016/j.canlet.2008.10.034.

[46] K.E. Pelka, K. Henn, A. Keck, B. Sapel, T. Braunbeck, Size does matter – Determination of the critical molecular size for the uptake of chemicals across the chorion of zebrafish (Danio rerio) embryos, Aquatic Toxicology 185 (2017) 1–10. https://doi.org/10.1016/j.aquatox.2016.12.015.

[47] S. Mitsuhashi, N. Matsuura, M. Ubukata, H. Oikawa, H. Shima, K. Kikuchi, Tautomycetin is a novel and specific inhibitor of serine/threonine protein phosphatase type 1, PP1, Biochem Biophys Res Commun 287 (2001) 328–331. https://doi.org/10.1006/bbrc.2001.5596.

[48] Y.M. Wee, M.Y. Choi, C.H. Kang, Y.H. Kim, J.H. Kim, S.K. Lee, S.Y. Yu, S.C. Kim, D.J. Han, The synergistic effect of tautomycetin on cyclosporine a-mediated immunosuppression in a rodent islet allograft model, Molecular Medicine 16 (2010) 298–306. https://doi.org/10.2119/molmed.2009.00099.

[49] P. Rashkov, I.P. Barrett, R.E. Beardmore, C. Bendtsen, I. Gudelj, Kinase Inhibition Leads to Hormesis in a Dual Phosphorylation-Dephosphorylation Cycle, PLoS Comput Biol 12 (2016). https://doi.org/10.1371/journal.pcbi.1005216.

[50] J.E. Walsh, M.R.I. Young, Interrelationship between protein phosphatase 1 and TGF-{beta} in regulating motility and cytoskeletal architecture of endothelial cells., Anticancer Res 30 (2010) 4861–6.

[51] J. Wang, C. Zhang, C. Li, D. Zhao, S. Li, L. Ma, Y. Cui, X. Wei, Y. Zhao, Y. Gao, MicroRNA-92a promotes vascular smooth muscle cell proliferation and migration through the ROCK/MLCK signalling pathway, J Cell Mol Med 23 (2019) 3696–3710. https://doi.org/10.1111/jcmm.14274.

[52] X. Zhou, Y. Liu, J. You, H. Zhang, X. Zhang, L. Ye, Myosin light-chain kinase contributes to the proliferation and migration of breast cancer cells through cross-talk with activated ERK1/2, Cancer Lett 270 (2008) 312–327. https://doi.org/10.1016/j.canlet.2008.05.028.

[53] Z.M. Wang, D.S. Yang, J. Liu, H.B. Liu, M. Ye, Y.F. Zhang, ROCK inhibitor Y-27632 inhibits the growth, migration, and invasion of Tca8113 and CAL-27 cells in tongue squamous cell carcinoma, Tumor Biology 37 (2016) 3757–3764. https://doi.org/10.1007/s13277-015-4115-6.

[54] T. Wang, W. Kang, L. Du, S. Ge, Rho-kinase inhibitor Y-27632 facilitates the proliferation, migration and pluripotency of human periodontal ligament stem cells, J Cell Mol Med 21 (2017) 3100–3112. https://doi.org/10.1111/jcmm.13222.

[55] K. Nagatoya, T. Moriyama, N. Kawada, M. Takeji, S. Oseto, T. Murozono, A. Ando, E. Imai, M. Hori, Y-27632 prevents tubulointerstitial fibrosis in mouse kidneys with unilateral ureteral obstruction., Kidney Int 61 (2002) 1684–95. https://doi.org/10.1046/j.1523-1755.2002.00328.x.

[56] M. Anis, J. Gonzales, R. Halstrom, N. Baig, C. Humpal, R. Demeritte, Y. Epshtein, J.R. Jacobson, D.R. Fraidenburg, Non-Muscle MLCK Contributes to Endothelial Cell Hyper-Proliferation through the ERK Pathway as a Mechanism for Vascular Remodeling in Pulmonary Hypertension, Int J Mol Sci 23 (2022). https://doi.org/10.3390/ijms232113641.

[57] L. Yin, K.I. Morishige, T. Takahashi, K. Hashimoto, S. Ogata, S. Tsutsumi, K. Takata, T. Ohta, J. Kawagoe, K. Takahashi, H. Kurachi, Fasudil inhibits vascular endothelial growth

factor-induced angiogenesis in vitro and in vivo, Mol Cancer Ther 6 (2007) 1517–1525. https://doi.org/10.1158/1535-7163.MCT-06-0689.

[58] T. Hu, C. Yang, M. Fu, J. Yang, R. Du, X. Ran, T. Yin, G. Wang, Cytotoxic effects of docetaxel as a candidate drug of drug-eluting stent on human umbilical vein endothelial cells and the signaling pathway of cell migration inhibition, adhesion delay and shape change, Regen Biomater 4 (2017) 167–178. https://doi.org/10.1093/rb/rbx010.

[59] G.P. Van Nieuw Amerongen, P. Koolwijk, A. Versteilen, V.W.M. Van Hinsbergh, Involvement of RhoA/Rho kinase signaling in VEGF-induced endothelial cell migration and angiogenesis in vitro, Arterioscler Thromb Vasc Biol 23 (2003) 211–217. https://doi.org/10.1161/01.ATV.0000054198.68894.88.

[60] Q. Wang, A. Fan, Y. Yuan, L. Chen, X. Guo, X. Huang, Q. Huang, Role of moesin in advanced glycation end products-induced angiogenesis of human umbilical vein endothelial cells, Sci Rep 6 (2016). https://doi.org/10.1038/srep22749.

[61] V. Hongisto, S. Jernström, V. Fey, J.P. Mpindi, K. Kleivi Sahlberg, O. Kallioniemi, M. Perälä, High-Throughput 3D Screening Reveals Differences in Drug Sensitivities between Culture Models of JIMT1 Breast Cancer Cells, PLoS One 8 (2013). https://doi.org/10.1371/journal.pone.0077232.

[62] K. Lawrenson, M. Notaridou, N. Lee, E. Benjamin, I.J. Jacobs, C. Jones, S.A. Gayther, In vitro three-dimensional modeling of fallopian tube secretory epithelial cells., BMC Cell Biol 14 (2013) 43. https://doi.org/10.1186/1471-2121-14-43.

[63] K. Tsuji-Tamura, M. Tamura, Basic fibroblast growth factor uniquely stimulates quiescent vascular smooth muscle cells and induces proliferation and dedifferentiation., FEBS Lett 596 (2022) 1686–1699. https://doi.org/10.1002/1873-3468.14345.

[64] K. Matsushita, S. Kobayashi, H. Akita, M. Konno, A. Asai, T. Noda, Y. Iwagami, T. Asaoka, K. Gotoh, M. Mori, Y. Doki, H. Eguchi, H. Ishii, Clinicopathological significance of MYL9 expression in pancreatic ductal adenocarcinoma, Cancer Rep 5 (2022). https://doi.org/10.1002/cnr2.1582.

[65] M. Feng, N. Dong, X. Zhou, L. Ma, R. Xiang, Myosin light chain 9 promotes the proliferation, invasion, migration and angiogenesis of colorectal cancer cells by binding to Yes-associated protein 1 and regulating Hippo signaling, Bioengineered 13 (2022) 96–106. https://doi.org/10.1080/21655979.2021.2008641.

[66] B. Kalyanaraman, Teaching the basics of cancer metabolism: Developing antitumor strategies by exploiting the differences between normal and cancer cell metabolism, Redox Biol 12 (2017) 833–842. https://doi.org/10.1016/j.redox.2017.04.018.

[67] B. Wen, L. Luo, Z. Zeng, X. Luo, MYL9 promotes squamous cervical cancer migration and invasion by enhancing aerobic glycolysis, Journal of International Medical Research 51 (2023). https://doi.org/10.1177/03000605231208582.

[68] J. Zhang, M. Betson, J. Erasmus, K. Zeikos, M. Bailly, L.P. Cramer, V.M.M. Braga, Actin at cell-cell junctions is composed of two dynamic and functional populations, J Cell Sci 118 (2005) 5549–5562. https://doi.org/10.1242/jcs.02639.

[69] C.K. Choi, M. Vicente-Manzanares, J. Zareno, L.A. Whitmore, A. Mogilner, A.R. Horwitz, Actin and α-actinin orchestrate the assembly and maturation of nascent adhesions in a myosin II motor-independent manner, 2008.

[70] C. Schwayer, M. Sikora, J. Slováková, R. Kardos, C.P. Heisenberg, Actin Rings of Power, Dev Cell 37 (2016) 493–506. https://doi.org/10.1016/j.devcel.2016.05.024.

[71] A.L. Miller, The contractile ring, Current Biology 21 (2011). https://doi.org/10.1016/j.cub.2011.10.044.

[72] I.M. Sehring, P. Recho, E. Denker, M. Kourakis, B. Mathiesen, E. Hannezo, B. Dong, D. Jiang, Assembly and positioning of actomyosin rings by contractility and planar cell polarity, (n.d.). https://doi.org/10.7554/eLife.09206.001.

[73] K. Tsuji, K. Uno, G.X. Zhang, M. Tamura, Periodontal ligament cells under intermittent tensile stress regulate mRNA expression of osteoprotegerin and tissue inhibitor of matrix metalloprotease-1 and -2, J Bone Miner Metab 22 (2004) 94–103. https://doi.org/10.1007/s00774-003-0456-0.

[74] M. Morioka, H. Parameswaran, K. Naruse, M. Kondo, M. Sokabe, Y. Hasegawa, B. Suki, S. Ito, Microtubule dynamics regulate cyclic stretch-induced cell alignment in human airway smooth muscle cells, PLoS One 6 (2011). https://doi.org/10.1371/journal.pone.0026384.

[75] A. Thomas, H. Daniel Ou-Yang, L. Lowe-Krentz, V.R. Muzykantov, Y. Liu, Biomimetic channel modeling local vascular dynamics of pro-inflammatory endothelial changes, Biomicrofluidics 10 (2016). https://doi.org/10.1063/1.4936672.

[76] A. Sarasa-Renedo, V. Tunç-Civelek, M. Chiquet, Role of RhoA/ROCK-dependent actin contractility in the induction of tenascin-C by cyclic tensile strain, Exp Cell Res 312 (2006) 1361–1370. https://doi.org/10.1016/j.yexcr.2005.12.025.

[77] B. Ladoux, R.M. Mège, X. Trepat, Front-Rear Polarization by Mechanical Cues: From Single Cells to Tissues, Trends Cell Biol 26 (2016) 420–433. https://doi.org/10.1016/j.tcb.2016.02.002.

[78] J.L. Tan, J. Tien, D.M. Pirone, D.S. Gray, K. Bhadriraju, C.S. Chen, Cells lying on a bed of microneedles: An approach to isolate mechanical force, Proceedings of the National Academy of Sciences 100 (2003) 1484–1489. https://doi.org/10.1073/pnas.0235407100.

[79] I. Baumgartner, A. Pieczek, O. Manor, ; Richard Blair, M. Kearney, K. Walsh, J.M. Isner, Constitutive Expression of phVEGF 165 After Intramuscular Gene Transfer Promotes Collateral Vessel Development in Patients With Critical Limb Ischemia, (1998). http://circ.ahajournals.org/.

[80] Y. Haibe, M. Kreidieh, H. El Hajj, I. Khalifeh, D. Mukherji, S. Temraz, A. Shamseddine, Resistance Mechanisms to Anti-angiogenic Therapies in Cancer, Front Oncol 10 (2020). https://doi.org/10.3389/fonc.2020.00221.

[81] D. Liang, J.R. Chang, A.J. Chin, A. Smith, C. Kelly, E.S. Weinberg, R. Ge, The role of vascular endothelial growth factor (VEGF) in vasculogenesis, angiogenesis, and hematopoiesis in zebrafish development, Mech Dev. 108 (2001) 29–43. www.elsevier.com/locate/modo.

[82] A. Nasevicius, J. Larson, S.C. Ekker, M. Beckman, S.C. Ekker, Distinct requirements for zebrafish angiogenesis revealed by a VEGF-A morphant, Yeast 17 (2000) 294–301. https://doi.org/10.1002/1097-0061(200012)17:4.

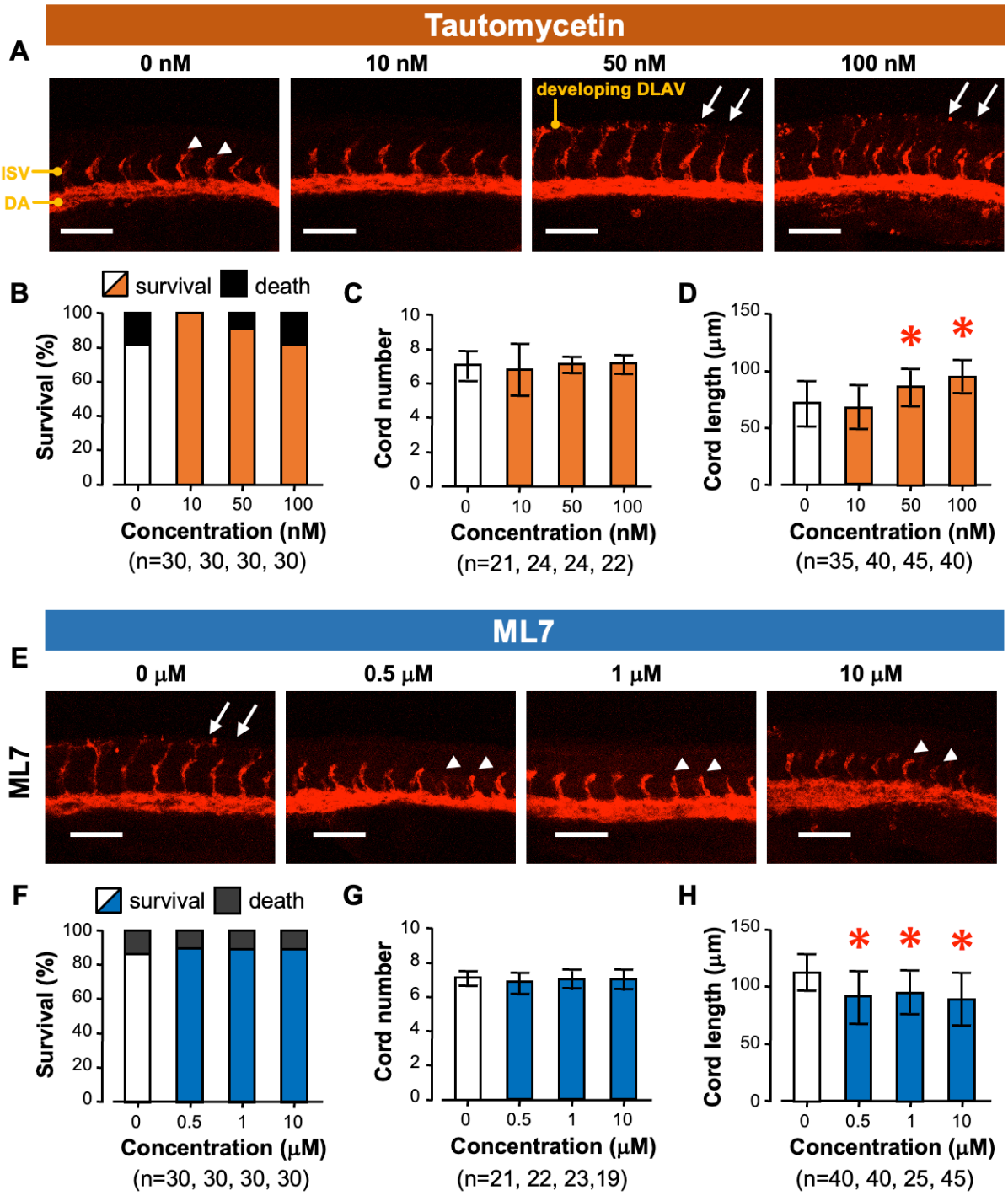
Tautomycetin
A
0 nM
10 nM
50 nM
100 nM
developing DLAV
ISV
DA
B
survival
death
Survival (%)
Concentration (nM)
(n=30, 30, 30, 30)
C
Cord number
Concentration (nM)
(n=21, 24, 24, 22)
D
Cord length (μm)
Concentration (nM)
(n=35, 40, 45, 40)
ML7
E
0 μM
0.5 μM
1 μM
10 μM
ML7
F
survival
death
Survival (%)
Concentration (μM)
(n=30, 30, 30, 30)
G
Cord number
Concentration (μM)
(n=21, 22, 23,19)
H
Cord length (μm)
Concentration (μM)
(n=40, 40, 25, 45)

Figure 1. Inhibition of PP1 and MLCK shows contrasting effects on vascular development in zebrafish embryos.

Tg(fli1a:Myr-mCherry) zebrafish embryos at 6 hpf were exposed to a protein phosphatase 1 (PP1) inhibitor tautomycetin (A–D) and a myosin light chain kinase (MLCK) inhibitor ML7 (E-H) at concentrations of 0, 10, 50, or 100 nM. Vascular structure in the middle trunk region was observed at 26 hours post-fertilization (hpf) (A–C) and 28 hpf (E–G). (A and E) Representative fluorescence images. ISV: intersegmental vessel, DA: dorsal aorta, DLAV: dorsal longitudinal anastomotic vessel. Scale bars indicate 100 μm. White arrowheads indicate the developing ISVs. White arrows indicate the ISVs that have reached the DLAV position. Similar results were obtained from three independent experiments. (B and F) The ratio of survived and dead embryos at 24 hpf. (C, G and D, H) The number (C and G) and the length (D and H) of ISVs. Error bars indicate mean SD. The results compared with the 0 nM control were analyzed by Dunnett's test (*$P < 0.05$). No significant difference was found in (C and G). The total number of embryos (B, C and F, G) and ISVs (D and H) measured in three independent experiments is indicated in the brackets.

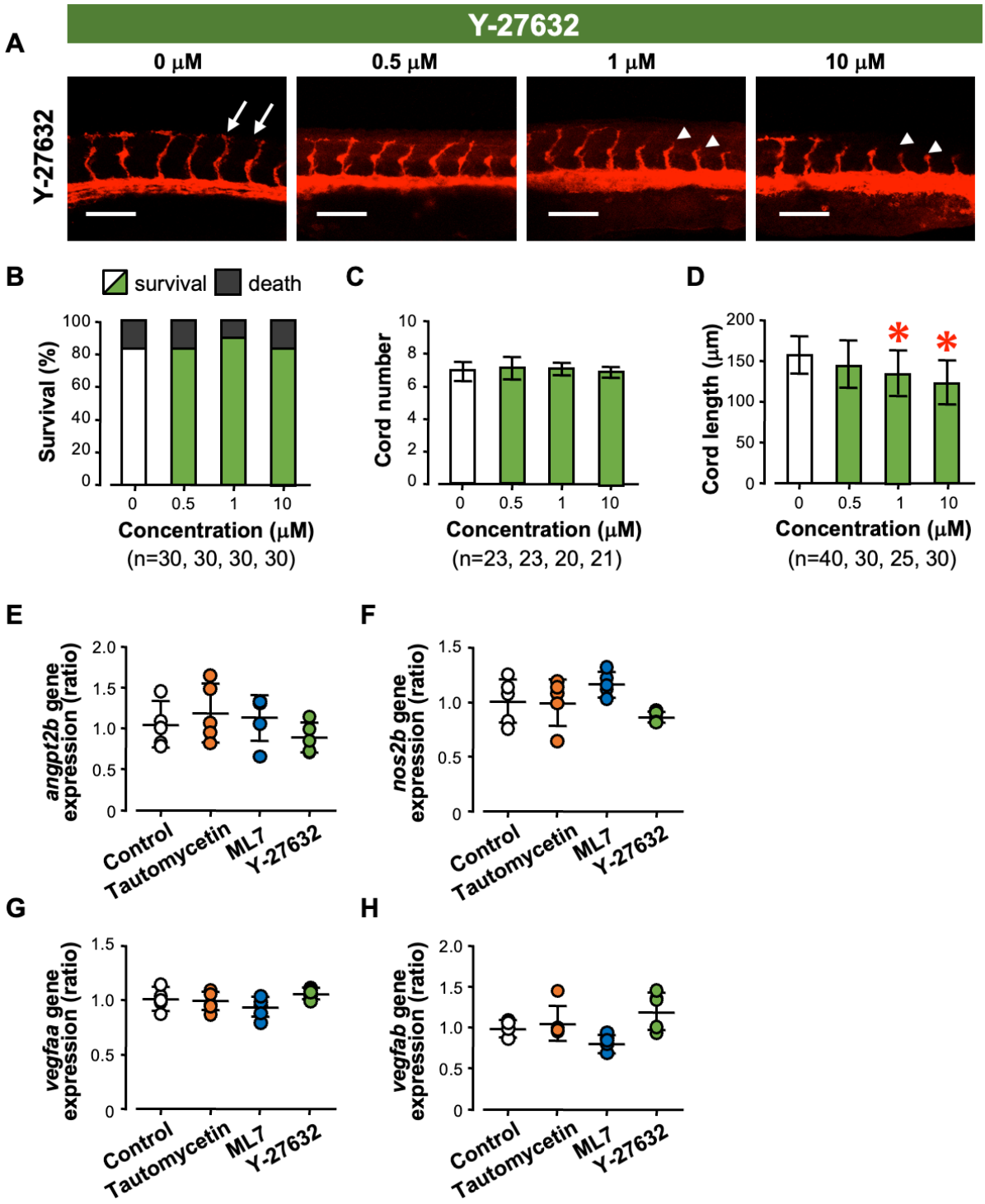
A
Y-27632
0 μM
0.5 μM
1 μM
10 μM
Y-27632
B
survival
death
Survival (%)
Concentration (μM)
(n=30, 30, 30, 30)
C
Cord number
Concentration (μM)
(n=23, 23, 20, 21)
D
Cord length (μm)
Concentration (μM)
(n=40, 30, 25, 30)
E
angpt2b gene expression (ratio)
F
nos2b gene expression (ratio)
G
vegfaa gene expression (ratio)
H
vegfab gene expression (ratio)
Control
Tautomycetin
ML7
Y-27632

Figure 2. Inhibition of ROCK suppresses vascular development in zebrafish embryos.
(A-D) *Tg(fli1a:Myr-mCherry)* zebrafish embryos at 6 hpf were exposed to a rho-associated coiled-coil forming kinase (ROCK) inhibitor Y-27632 at concentrations of 0, 0.5, 1, or 10 μM. Vascular structure in the middle trunk region was observed at 28 hpf. (A) Representative fluorescence images. Scale bars indicate 100 μm. White arrows indicate the ISVs that have reached the DLAV. White arrowheads indicate the developing ISVs. Similar results were obtained from three independent experiments. (B) The ratio of survived and dead embryos at 24 hpf (C and D). The number (C) and the length (D) of ISVs. Error bars indicate mean SD. The results compared with the 0 μM control were analyzed by Dunnett's test (*$P < 0.05$). No significant difference was found in (C). The total number of embryos (B and C) and ISVs (D) measured in three independent experiments is indicated in the brackets. (E-H) *Tg(fli1a:Myr-mCherry)* zebrafish embryos at 6 hpf were exposed to 100 nM of tautomycetin, 10 μM of ML7, and 10 μM of Y-27632. At 28 hpf, the total RNA was extracted and applied for analysis using real-time PCR. Expression levels of the target genes normalized by *actb1* expression are presented as a fold change relative to the control. Error bars indicate mean SD. The results were analyzed by Dunnett's test ($n = 5$ from five independent experiments). No statistically significant differences were found in any of the comparisons (E–H).

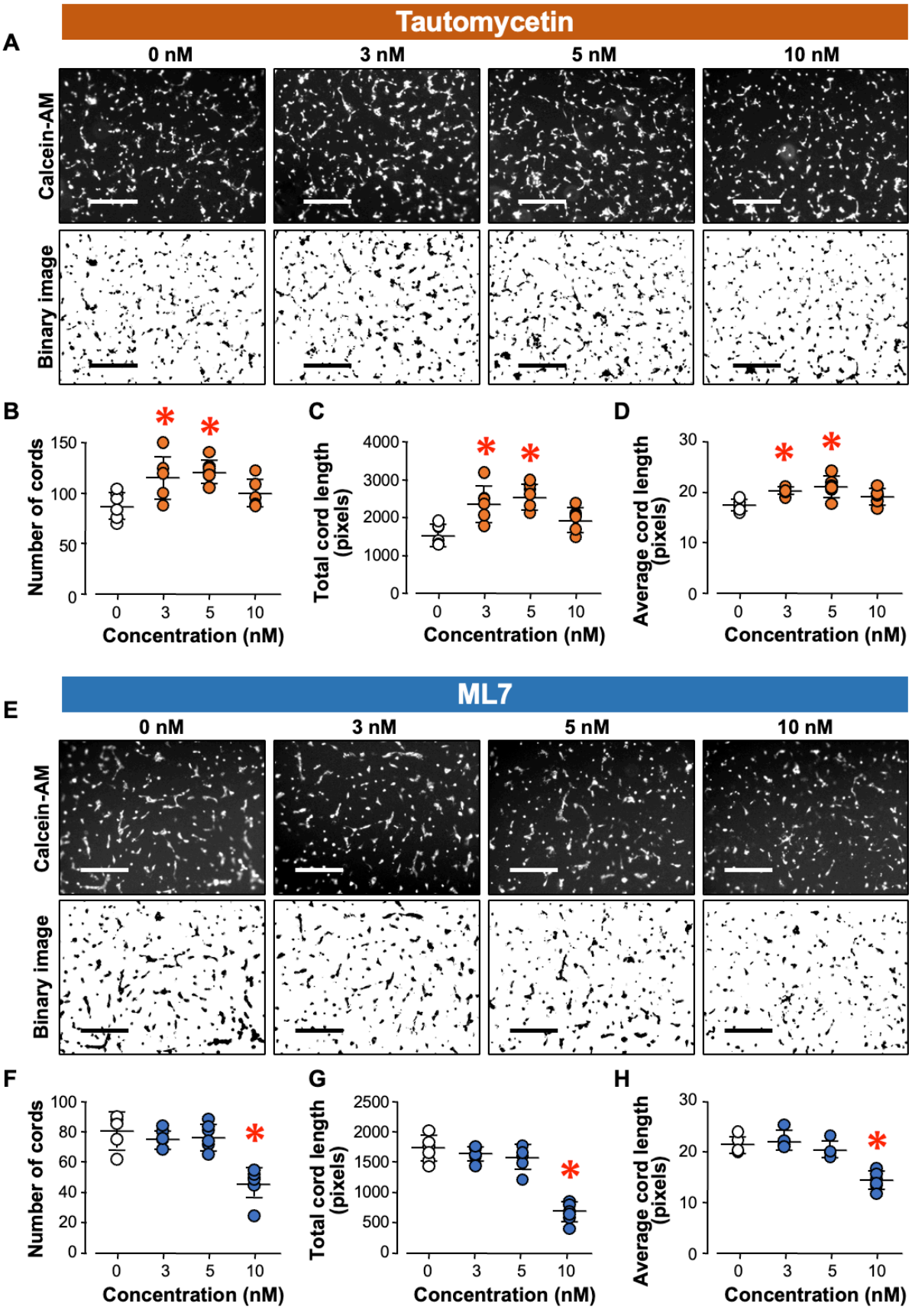
Tautomycetin
A
0 nM
3 nM
5 nM
10 nM
Calcein-AM
Binary image
B
Number of cords
Concentration (nM)
C
Total cord length (pixels)
Concentration (nM)
D
Average cord length (pixels)
Concentration (nM)
ML7
E
0 nM
3 nM
5 nM
10 nM
Calcein-AM
Binary image
F
Number of cords
Concentration (nM)
G
Total cord length (pixels)
Concentration (nM)
H
Average cord length (pixels)
Concentration (nM)

Figure 3. Inhibition of PP1 and MLCK shows contrasting effects on angiogenesis in human ECs. In type I collagen gel 3D sandwich culture containing VEGF-A165 (10 ng/ml), human umbilical vein endothelial cells (HUVECs) were treated with tautomycetin (A–D) and ML7 (E–H) at concentrations of 0, 3, 5, or 10 nM for 2 days. (A and E) Vascular cord formation. Representative fluorescence images with calcein-AM (upper) and binary images (lower) of cord structures. Scale bars indicate 500 μm. (B–D and F–H) The number (B and F) and total length (C and G) of cord structures, and the average cord length (D and H) per field. Error bars indicate mean SD. The results compared with the 0 nM control were analyzed by Dunnett's test (n = 6 fields, *P < 0.05). Similar results were obtained in three independent experiments.

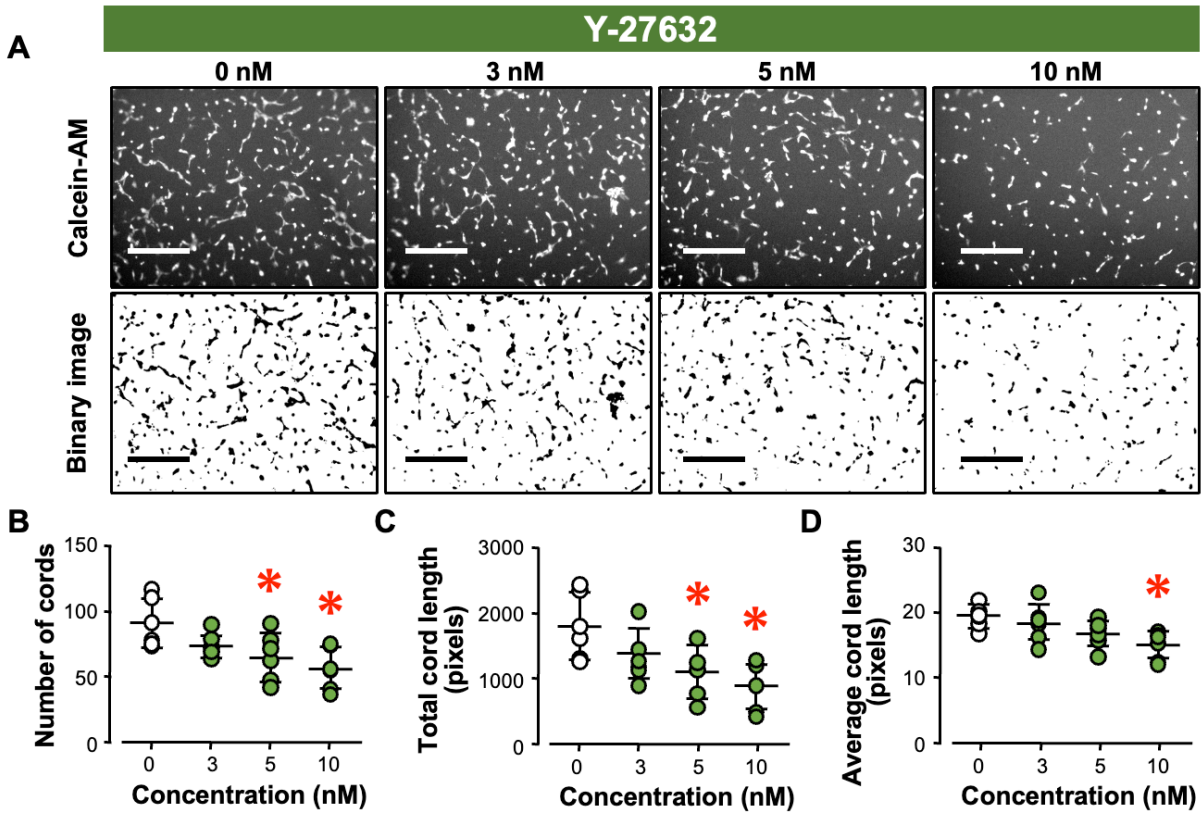

Figure 4. Inhibition of ROCK suppresses angiogenesis in human ECs.

In type I collagen gel sandwich culture containing VEGF-A165 (10 ng/ml), HUVECs were treated with Y-27632 at concentrations of 0, 3, 5, or 10 nM for 2 days. (A) Vascular cord formation. Representative fluorescence images with calcein-AM (upper) and binary images (lower) of cord structures. Scale bars indicate 500 μm. (B–D) The number (B) and total length (C) of cord structures, and the average cord length (D) per field. Error bars indicate mean SD. The results compared with the 0 nM control were analyzed by Dunnett's test (n = 6 fields, *P < 0.05). Similar results were obtained in three independent experiments.

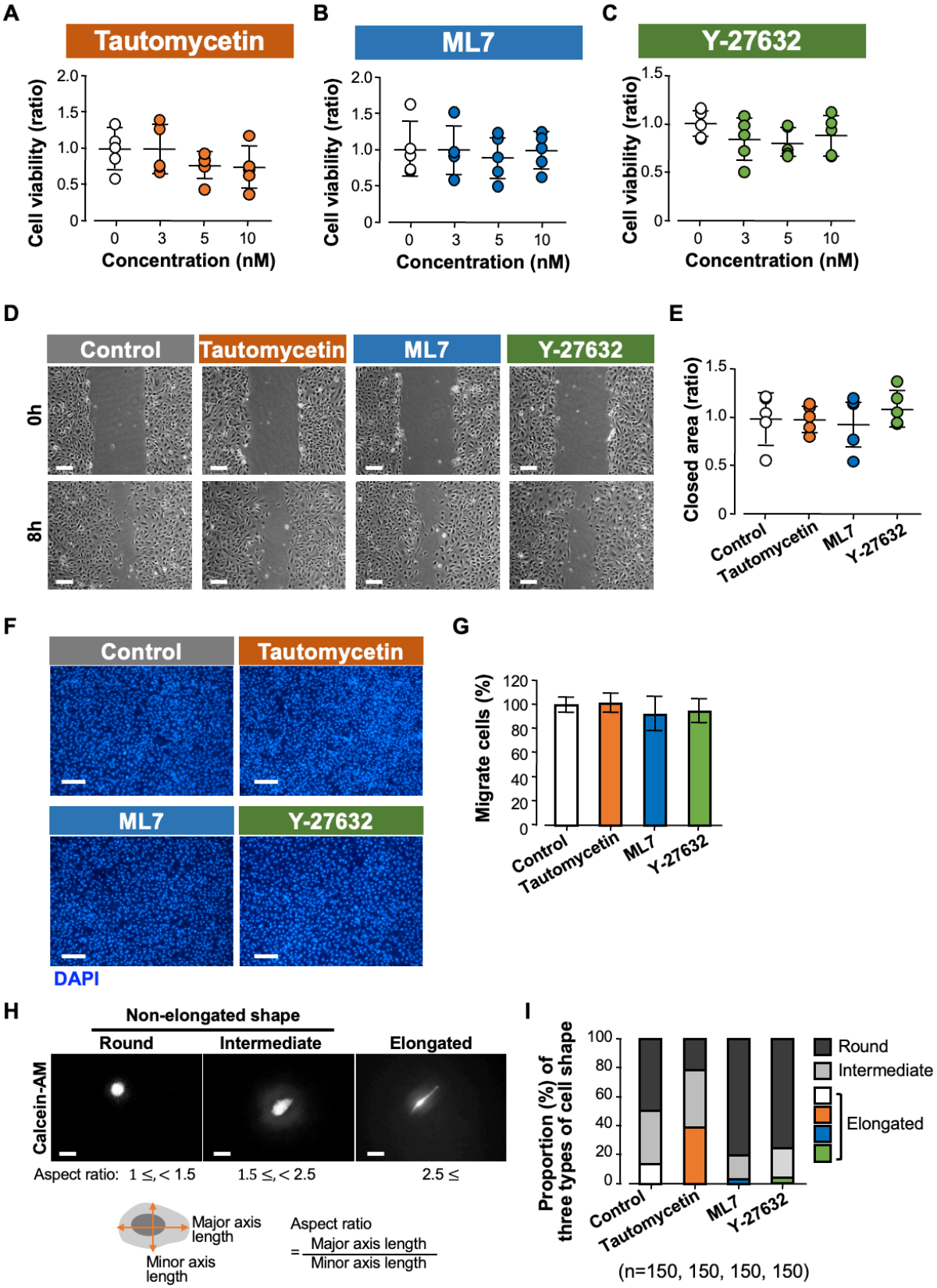
A
Tautomycetin
Cell viability (ratio)
2.0
1.5
1.0
0.5
0
0
3
5
10
Concentration (nM)
B
ML7
Cell viability (ratio)
2.0
1.5
1.0
0.5
0
0
3
5
10
Concentration (nM)
C
Y-27632
Cell viability (ratio)
1.5
1.0
0.5
0
0
3
5
10
Concentration (nM)
D
Control
Tautomycetin
ML7
Y-27632
0h
8h
E
Closed area (ratio)
1.5
1.0
0.5
0
Control
Tautomycetin
ML7
Y-27632
F
Control
Tautomycetin
ML7
Y-27632
DAPI
G
Migrate cells (%)
120
100
80
60
40
20
0
Control
Tautomycetin
ML7
Y-27632
H
Non-elongated shape
Round
Intermediate
Elongated
Calcein-AM
Aspect ratio: 1 ≤, < 1.5
1.5 ≤, < 2.5
2.5 ≤
Major axis length
Minor axis length
Aspect ratio
= Major axis length / Minor axis length
I
Proportion (%) of three types of cell shape
100
80
60
40
20
0
Control
Tautomycetin
ML7
Y-27632
Round
Intermediate
Elongated
(n=150, 150, 150, 150)

Figure 5. Inhibition of PP1 and MLCK affects cell morphology, but not cell viability or migration

(A-C) Cell viability assay was performed in HUVECs treated with tautomycetin (A), ML7 (B), and Y-27632 (C) at concentrations of 0, 3, 5, or 10 nM for 2 days. The cell viability is presented as a ratio relative to the 0 nM control. Error bars indicate mean SD. Data were analyzed using Dunnett's test (n = 5). No significant difference was found in all experiments, compared with the control. Similar results were obtained in three independent experiments. (D and E) Migration assay by scratch-wound method was performed in monolayers of HUVECs treated with 3 nM of tautomycetin, 10 nM of ML7, and 10 nM of Y-27632 for 8 h. (D) Images at 0 h and 8 h after scratching. Scale bars indicate 200 μm. Similar results were obtained in three independent experiments. (E) Closed area for migration ability is presented as a ratio relative to the control. Error bars indicate mean SD. Data were analyzed using Dunnett's test (n = 5). No significant difference was found in all experiments, compared with the control. (F and G) Migration assay using transwell insert system was performed in HUVECs. Cells were seeded on the upper side of the transwell insert filled with basal medium, and the lower chamber was filled with growth medium containing 10 ng/ml VEGF-A165 with 3 nM of tautomycetin, 10 nM of ML7, and 10 nM of Y-27632. Cells were allowed to migrate into the bottom of the insert membrane for 6 h. (F) Nuclear DAPI staining of the migrate cells. Scale bars indicate 200 μm. (G) Relative ratio of migrate cells per field. Error bars indicate mean SD. Data were analyzed using Dunnett's test (n = 5). No significant difference was found in all experiments, compared with the control. Similar results were obtained in three independent experiments. (H and I) Cell morphology analysis was performed in HUVECs maintained in type I collagen gel 3D cultures containing VEGF-A165 (10 ng/ml), and added 3 nM of tautomycetin, 10 nM of ML7, or 10 nM of Y-27632 for 2 days. (H) Images of three types of EC shapes are shown: the "round" and "intermediate" non-elongated shapes, and the "elongated" shape, which are defined by their aspect ratio (each range is shown below). Scale bars indicate 40 μm. Similar results were obtained in three independent experiments. The lower panel is a schematic representation of cellular aspect ratio determination. (I) The proportion of the three types of EC shapes. The total number of ECs indicated in the brackets was obtained from three independent experiments.

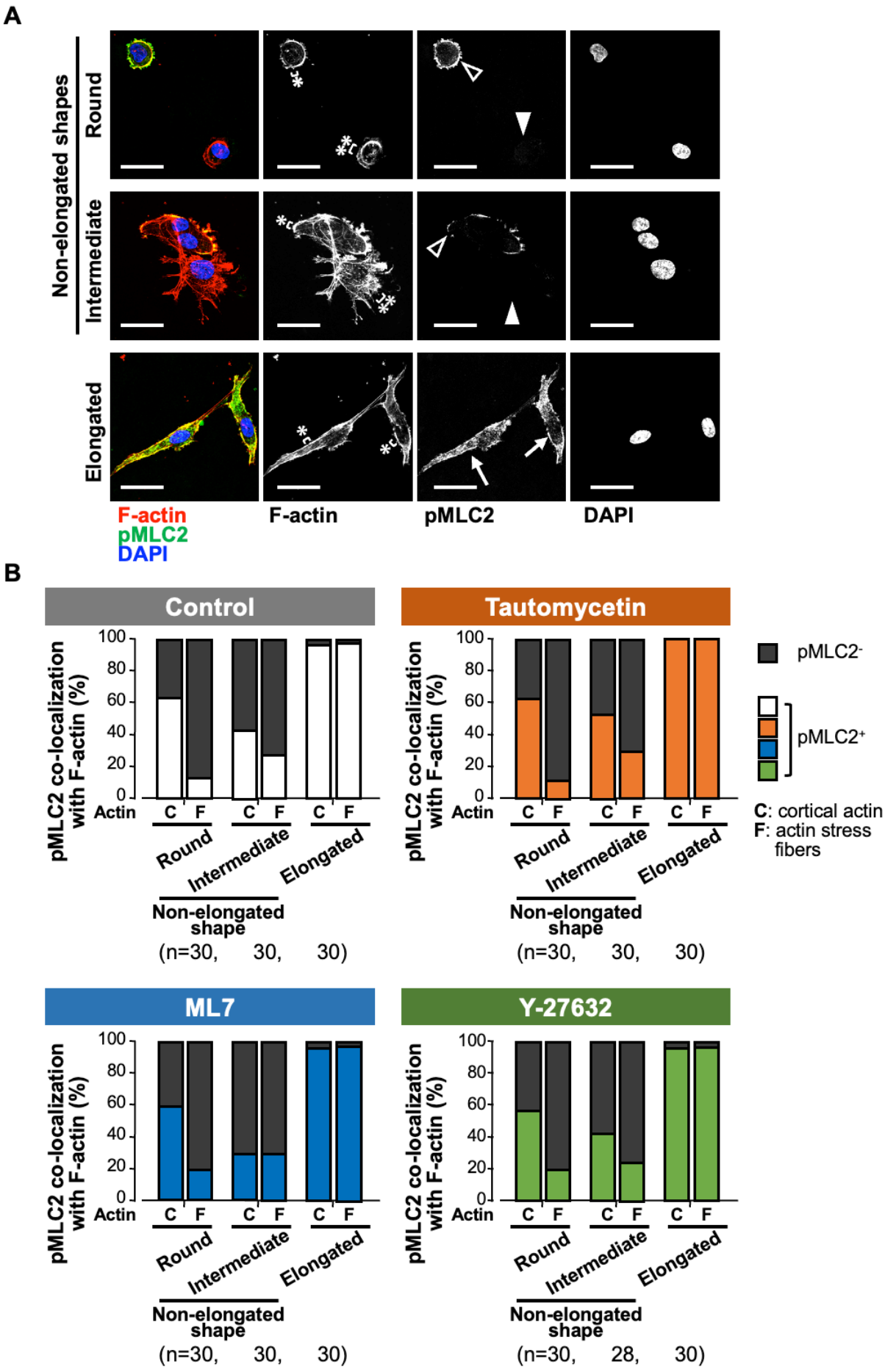
A
Non-elongated shapes
Round
Intermediate
Elongated
F-actin
pMLC2
DAPI
F-actin
pMLC2
DAPI
B
Control
Tautomycetin
ML7
Y-27632
pMLC2 co-localization with F-actin (%)
100
80
60
40
20
0
Actin
C F C F C F
Round
Intermediate
Elongated
Non-elongated shape
(n=30, 30, 30)
(n=30, 28, 30)
pMLC2-
pMLC2+
C: cortical actin
F: actin stress fibers

Figure 6. EC elongation is accompanied by interaction between F-actin and pMLC2.
Localization analysis of F-actin and pMLC2 was performed in HUVECs maintained in type I collagen gel 3D cultures containing VEGF-A165 (10 ng/ml) for 2 days. (A) Fluorescent images after staining with F-actin (red), pMLC2 (green) and DAPI (blue). Images of three types of EC shapes are shown: the "round" and "intermediate" non-elongated shapes, and the "elongated" shape. Scale bars show 30 μm. A single asterisk indicates tightly arranged cortical actin. Double asterisks indicate loosely arranged cortical actin. White edged arrowheads indicate "non-elongated shapes" of ECs with cortical actin that was co-localized with pMLC2 and actin stress fibers that were not co-localized with pMLC2. White arrowheads indicate "non-elongated shapes" of ECs with actin structures that were not co-localized with pMLC2. White arrows indicate "elongated shape" of ECs with cortical actin and actin stress fibers that were co-localized with pMLC2. Similar results were observed in three independent experiments. (B) Co-localization analysis of pMLC2 with cortical actin and actin stress fibers in three types of EC shape. The total number of ECs indicated in the brackets was obtained from three independent experiments.

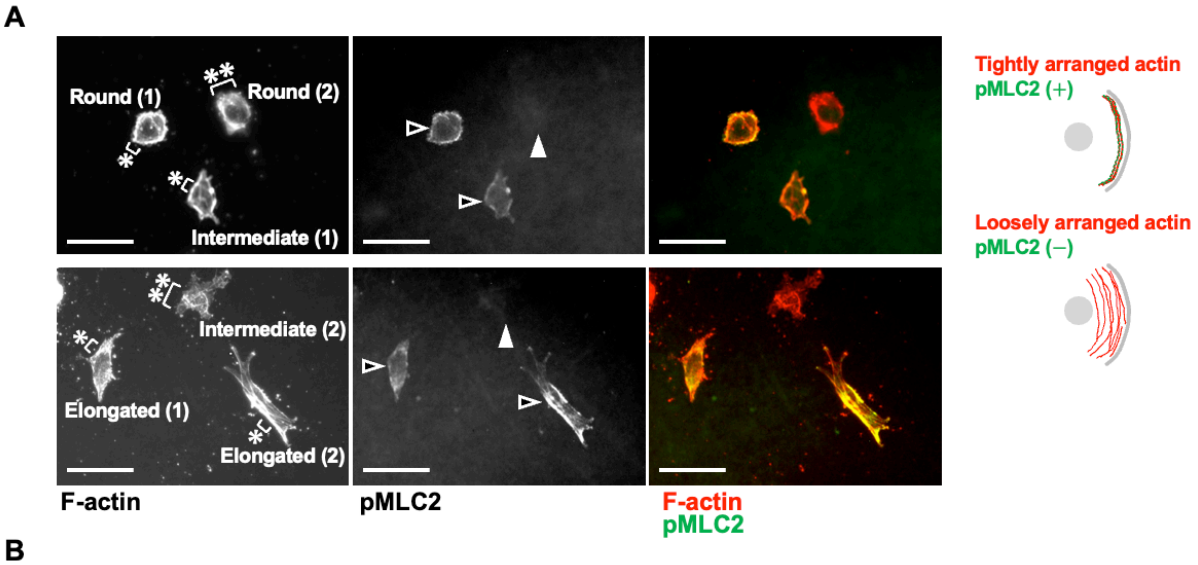
A
Round (1)
Round (2)
Intermediate (1)
Intermediate (2)
Elongated (1)
Elongated (2)
F-actin
pMLC2
F-actin
pMLC2
Tightly arranged actin
pMLC2 (+)
Loosely arranged actin
pMLC2 (−)

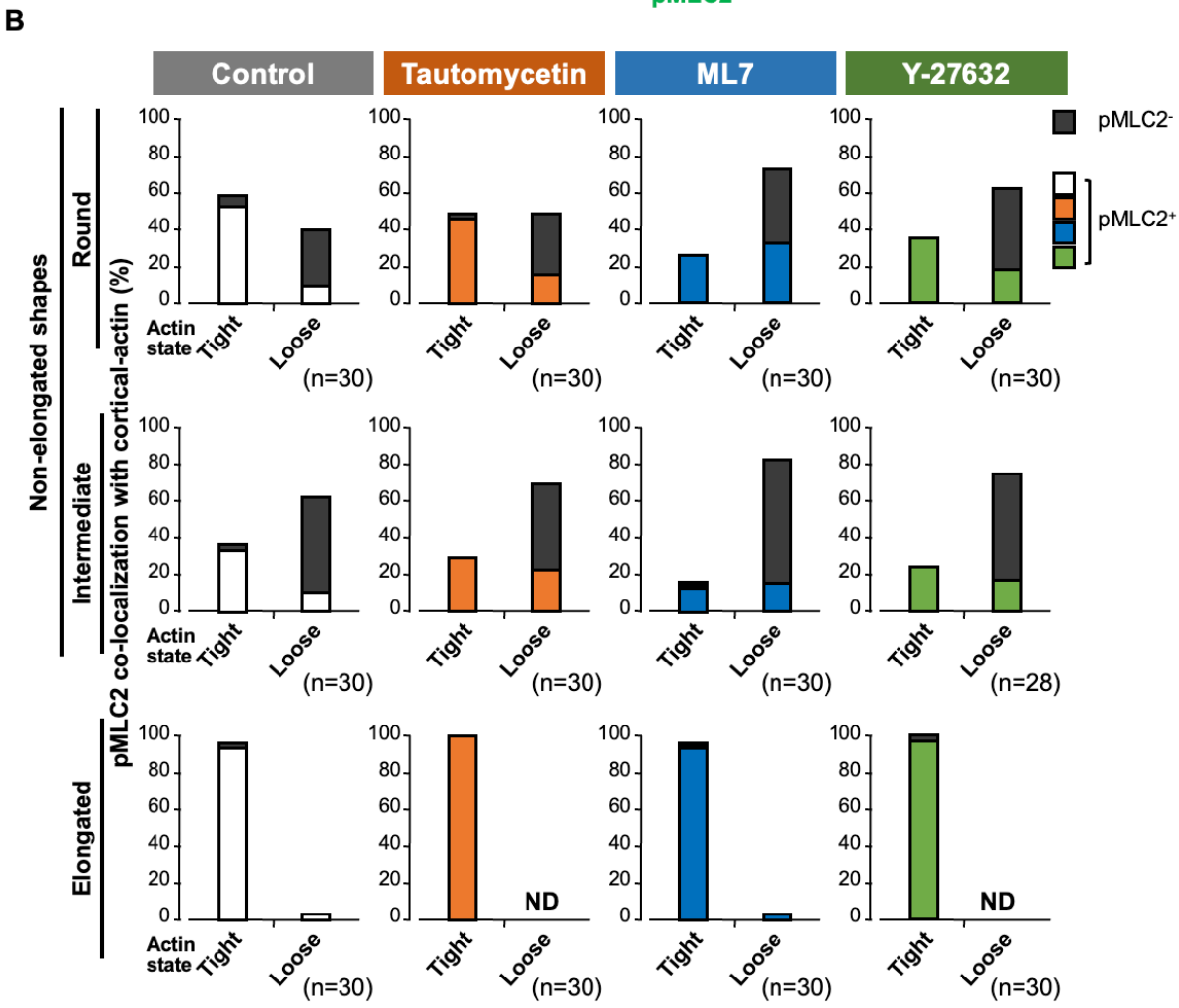
B
Control
Tautomycetin
ML7
Y-27632
pMLC2-
pMLC2+
Non-elongated shapes
Round
Intermediate
Elongated
pMLC2 co-localization with cortical-actin (%)
Actin state
Tight
Loose
(n=30)
(n=28)
ND

Figure 7. Tightly arrangement of actin filaments is associated with pMLC2

Analysis of F-actin arrangement and pMLC2 co-localization was performed in HUVECs maintained in type I collagen gel 3D cultures containing VEGF-A165 (10 ng/ml) for 2 days. (A) Fluorescent images after staining with F-actin and pMLC2. Images of three types of EC shapes are shown: the "round" and "intermediate" non-elongated shapes, and the "elongated" shape. Scale bars show 50 μm. A single asterisk indicates tightly arranged cortical actin. Double asterisks indicate loosely arranged cortical actin. White edged arrowheads indicate ECs with cortical actin co-localized with pMLC2. White arrowheads indicate ECs with cortical actin not co-localized with pMLC2. Round (1) and Intermediate (1) show tight actin bundles with pMLC2. Round (2) and Intermediate (2) show loosely arranged actin without pMLC2. Elongated (1) and (2) show tight actin bundles with pMLC2. Similar results were observed in three independent experiments. Right, schematic model indicates tightly arranged actin co-localized with pMLC2, and loosely arranged actin non-co-localized with pMLC2. (B) Co-localization analysis of pMLC2 with tightly and loosely arranged cortical actin in three types of EC shape. *ND* not detected. The total number of ECs indicated in the brackets was obtained from three independent experiments.

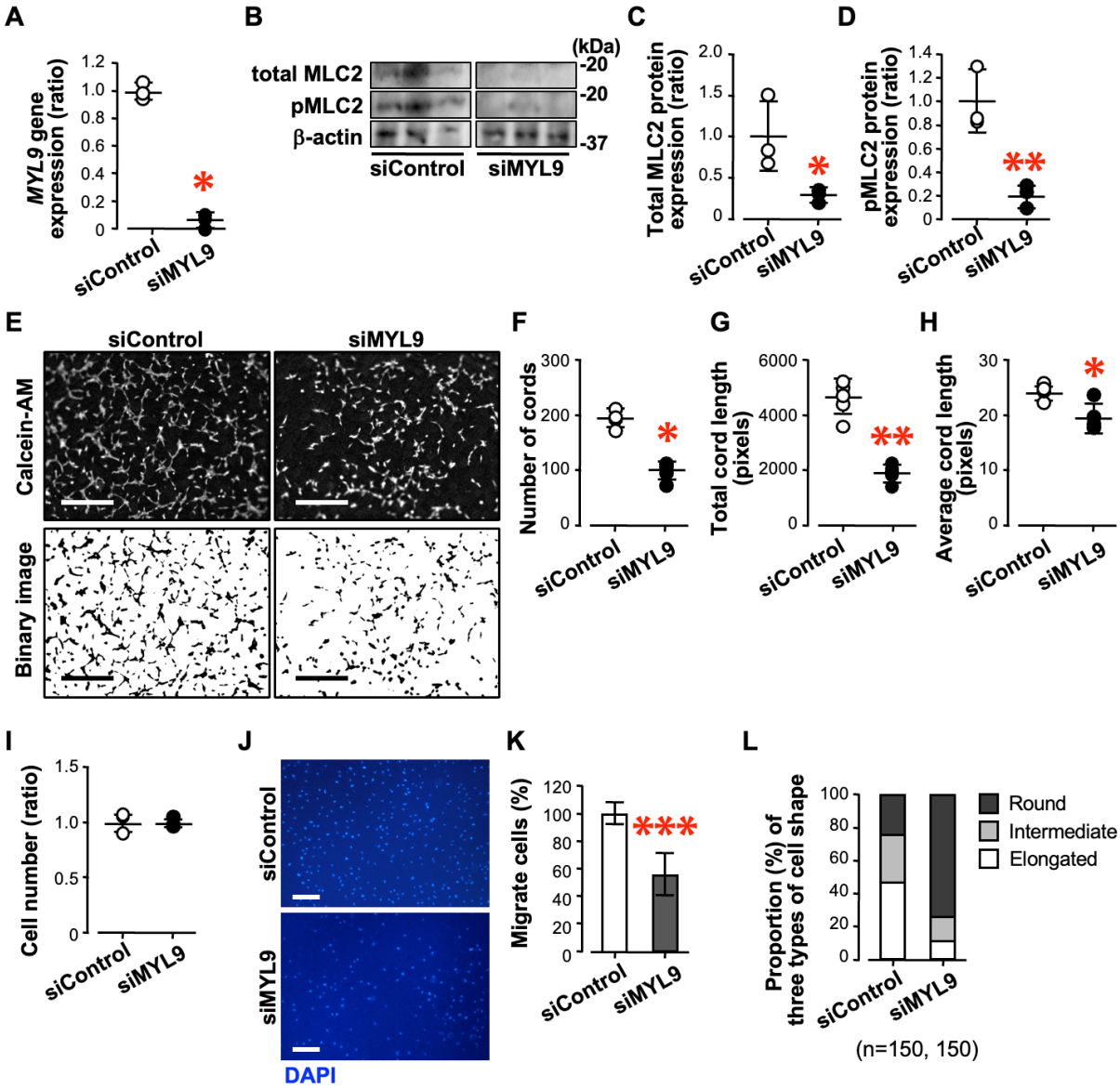
A
MYL9 gene expression (ratio)
1.2
1.0
0.8
0.6
0.4
0.2
0
*
siControl
siMYL9
B
(kDa)
total MLC2
pMLC2
β-actin
-20
-20
-37
siControl
siMYL9
C
Total MLC2 protein expression (ratio)
2.0
1.5
1.0
0.5
0
*
siControl
siMYL9
D
pMLC2 protein expression (ratio)
1.4
1.2
1.0
0.8
0.6
0.4
0.2
0
**
siControl
siMYL9
E
siControl
siMYL9
Calcein-AM
Binary image
F
Number of cords
300
200
100
0
*
siControl
siMYL9
G
Total cord length (pixels)
6000
4000
2000
0
**
siControl
siMYL9
H
Average cord length (pixels)
30
20
10
0
*
siControl
siMYL9
I
Cell number (ratio)
1.5
1.0
0.5
0
siControl
siMYL9
J
siControl
siMYL9
DAPI
K
Migrate cells (%)
120
100
80
60
40
20
0
***
siControl
siMYL9
L
Proportion (%) of three types of cell shape
100
80
60
40
20
0
Round
Intermediate
Elongated
siControl
siMYL9
(n=150, 150)

Figure 8. Knockdown of MYL9 gene encoding MLC2 suppresses angiogenesis in human ECs. HUVECs were transfected with MYL9 siRNA (100 nM), or control siRNA (100 nM), which indicated as follows: siMYL9 and siControl. (A) The MYL9 mRNA expression level at 1 day after transfection was analyzed using real-time quantitative PCR analysis. Expression levels normalized by *ACTB* are presented as a fold change relative to siControl. Error bars indicate mean SD. The results were analyzed an F-test followed by an unpaired, two-tailed t-test (n = 3, *P < 0.05). Similar results were obtained from three independent experiments. (B-D) The total MLC2 and pMLC2 protein expression levels at 2 days after transfection was analyzed using a western blot analysis. (B) Western blot images. The comparable band images of siControl and siMYL9 are from the same single western blot image. (C) Expression levels normalized by β-actin are presented as a fold change relative to siControl. Error bars indicate mean SD. The results were analyzed an F-test followed by an unpaired, two-tailed t-test (n = 3 from three independent experiments, *P < 0.05, **P < 0.01). (E-H) Cells were maintained in type I collagen gel sandwich culture containing VEGF-A165 (10 ng/ml) for 2 days. (E) Vascular cord formation. Representative fluorescence images with calcein-AM (upper) and binary images (lower) of cord structures. Scale bars indicate 500 μm. (F–H) The number (F) and total length (G) of cord structures, and the average cord length (H) per field. Error bars indicate mean SD. The results were analyzed an F-test followed by an unpaired, two-tailed t-test (n = 5, *P < 0.05, **P < 0.01). Similar results were obtained in three independent experiments. (I) Cell number was counted manually at 2 days after transfection and presented as a ratio relative to siControl. Error bars indicate mean SD. The results were analyzed an F-test followed by an unpaired, two-tailed t-test (n = 3). No significant difference was found. Similar results were obtained in three independent experiments. (J and K) Migration assay using transwell insert system was performed at 1 day after transfection. Cells were seeded on the upper side of the transwell insert filled with basal medium, and the lower chamber was filled with growth medium containing VEGF-A165 (10 ng/ml). Cells were allowed to migrate to the bottom of the insert membrane for 6 h. (J) Nuclear DAPI staining of the migrate cells. Scale bars indicate 200 μm. (K) Relative ratio of migrate cells per field. Error bars indicate mean SD. The results were analyzed an F-test followed by an unpaired, two-tailed t-test (n = 5, ***P < 0.001). Similar results were obtained in three independent experiments. (L) Cell morphology analysis was performed in cells maintained in type I collagen gel 3D cultures containing VEGF-A165 (10 ng/ml) for 2 days, as described in Figure 5H. The proportion of the three types of cell shapes are presented. The total number of cells indicated in the brackets was obtained from three independent experiments.

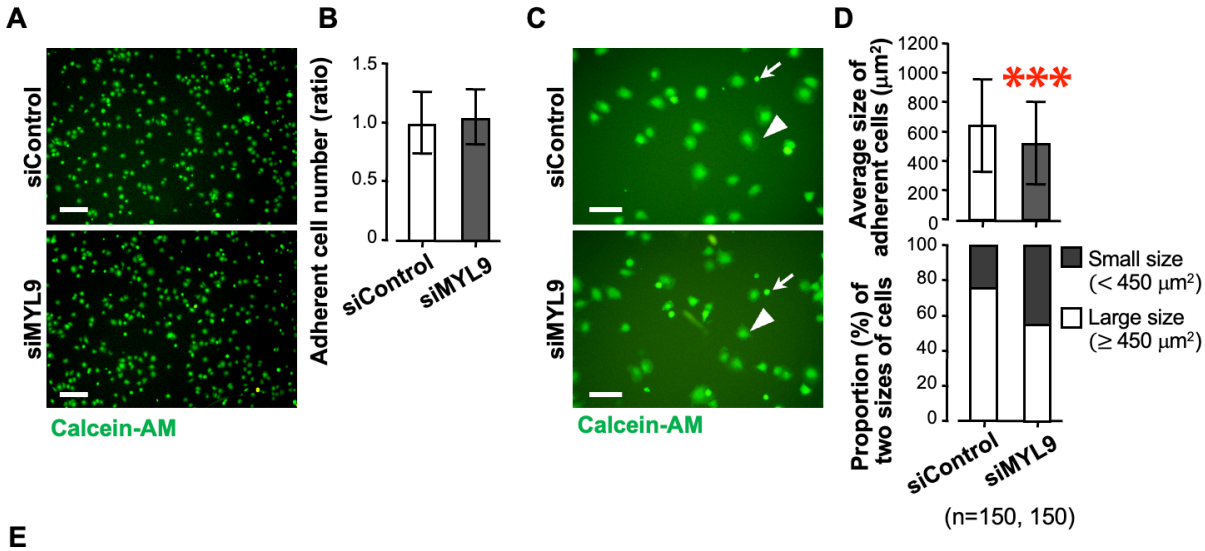
A
siControl
siMYL9
Calcein-AM
B
Adherent cell number (ratio)
1.5
1.0
0.5
0
siControl
siMYL9
C
siControl
siMYL9
Calcein-AM
D
Average size of adherent cells (μm²)
1200
1000
800
600
400
200
0
***
Proportion (%) of two sizes of cells
100
80
60
40
20
0
Small size (< 450 μm²)
Large size (≥ 450 μm²)
siControl
siMYL9
(n=150, 150)

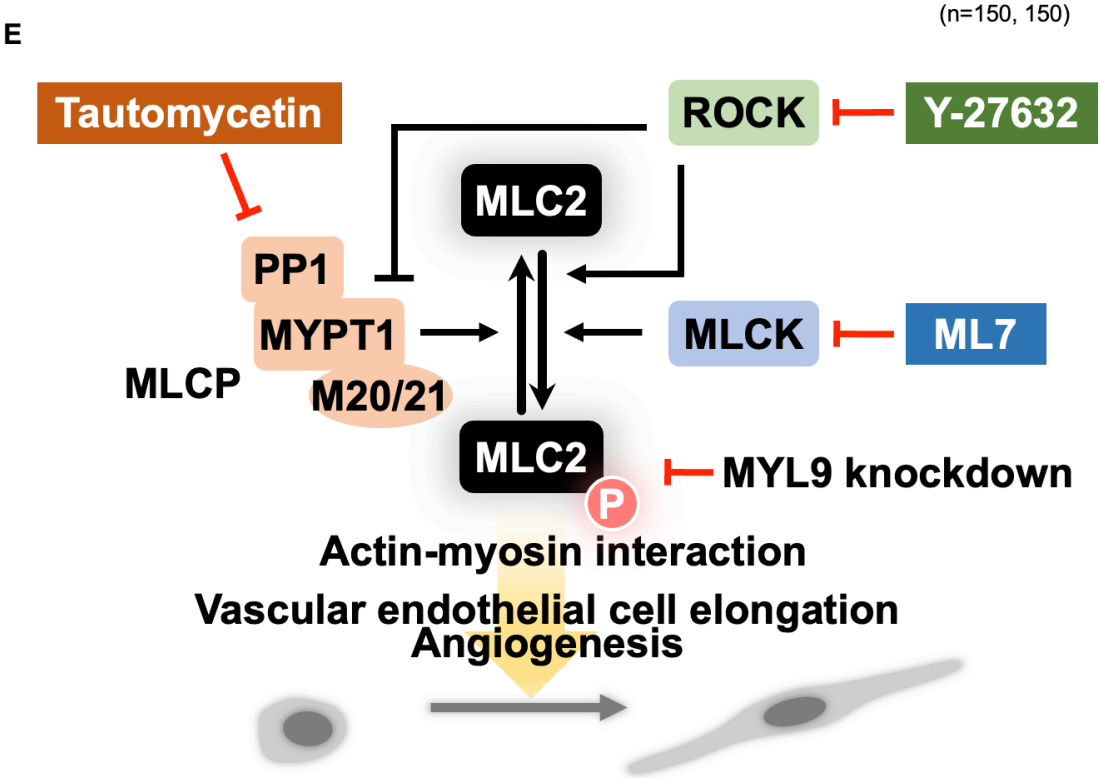
E
Tautomycetin
ROCK
Y-27632
MLC2
PP1
MYPT1
MLCP
M20/21
MLCK
ML7
MLC2
P
MYL9 knockdown
Actin-myosin interaction
Vascular endothelial cell elongation
Angiogenesis

Figure 9. Knockdown of MYL9 gene inhibits cell spreading of human ECs.

(A-D) Cell adhesion and spreading assay was performed in HUVECs 1 day after transfection with MYL9 siRNA, or control siRNA. Cells detached by trypsin treatment were allowed to adhere to gelatin-coated film bottom plates for 1 h. (A and B) Analysis of adherent cell numbers. (A) Calcein-AM fluorescence images of adherent cells. Scale bars indicate 200 μm. (B) The number of adherent cells per field is presented as a ratio relative to siControl. Error bars indicate mean SD. The results were analyzed an F-test followed by an unpaired, two-tailed t-test (n = 15). No significant difference was found. Similar results were obtained in three independent experiments. (C and D) Analysis of adherent cell size. (C) Calcein-AM fluorescence images of adherent cells. Scale bars indicate 90 μm. White arrows indicate the "small size" of cells". White arrowheads indicate the "large size" of cells. (D) The average size of adherent cells (upper panel) and the proportion of the two types of adherent cell size (lower panel). The total number of cells indicated in the brackets. In the upper panel, error bars indicate mean SD, and the results were analyzed an F-test followed by an unpaired, two-tailed t-test (***$P < 0.001$). Similar results were obtained in three independent experiments. (E) Schematic model for control of angiogenesis via phosphorylation of MLC2. Phosphorylation of MLC2 by MLCK or ROCK signaling stimulates actin-myosin interaction, leading to angiogenesis associated with vascular endothelial elongation. MLCP, a holoenzyme comprised of a PP1 catalytic subunit, regulatory subunit MYPT1 and M20/M21, dephosphorylates pMLC2, and its activity is inhibited by ROCK signaling. Inhibition of PP1 by tautomycetin probably inactivates MLCP, thereby inhibiting the dephosphorylation of pMLC2. MLCK Inhibition by ML7 and ROCK inhibition by Y-27632 suppresses phosphorylation of MLC2. Knockdown of the MYL9, the gene encoding the MLC2 protein, suppresses phosphorylation of MLC2 along with total MLC2. MLCP: myosin light chain phosphatase, PP1: protein phosphatase 1, MYPT1: myosin phosphatase targeting subunit 1, MLC2: Myosin regulatory light chain 2, ROCK: Rho/Rho associated coiled coil-forming protein kinase, MLCK: myosin light-chain kinase.

Supplementary Table1. Shape descriptors of vascular endothelial cells. HUVECs were cultured in type I collagen gel 3D cultures containing VEGF-A165 (10 ng/ml), and treated with 3 nM of tautomycetin, 10 nM of ML7, or 10 nM of Y-27632 for 2 days.

Inhibitor	Aspect ratio	Circularity	Roundness
Control	1.785±0.808	0.884±0.132	0.647±0.213
Tautomycetin	2.545±1.338*	0.77±0.182*	0.489±0.214*
ML7	1.339±0.385*	0.957±0.066*	0.792±0.166*
Y-27632	1.389±0.435*	0.95±0.072*	0.768±0.17*

The results compared with control were analyzed by Dunnett's test (*P < 0.05, n=150 in three independent experiments.

Supplementary Table2. Shape descriptors of MYL9-knockdown vascular endothelial cells. MYL9-knockdown HUVECs (siMYL9) were cultured in type I collagen gel 3D cultures containing VEGF-A165 (10 ng/ml)

	Aspect ratio	Circularity	Roundness
siControl	2.598±1.128	0.75±0.175	0.468±0.216
siMYL9	1.407±0.575***	0.941±0.098***	0.787±0.203***

The results compared with the control (siControl) were analyzed by an F-test followed by an unpaired, two-tailed t-test (***P < 0.001, n=150 in three independent experiments.)

Supplementary information

Title: Pharmacological control of angiogenesis by regulating phosphorylation of myosin light chain 2

Kiyomi Tsuji-Tamura*, Mari Sato, and Masato Tamura

[1]Oral Biochemistry and Molecular Biology, Department of Oral Health Science, Faculty of Dental Medicine and Graduate School of Dental Medicine, Hokkaido University, Kita 13, Nishi 7, Kita-Ku, Sapporo 060-8586, Japan

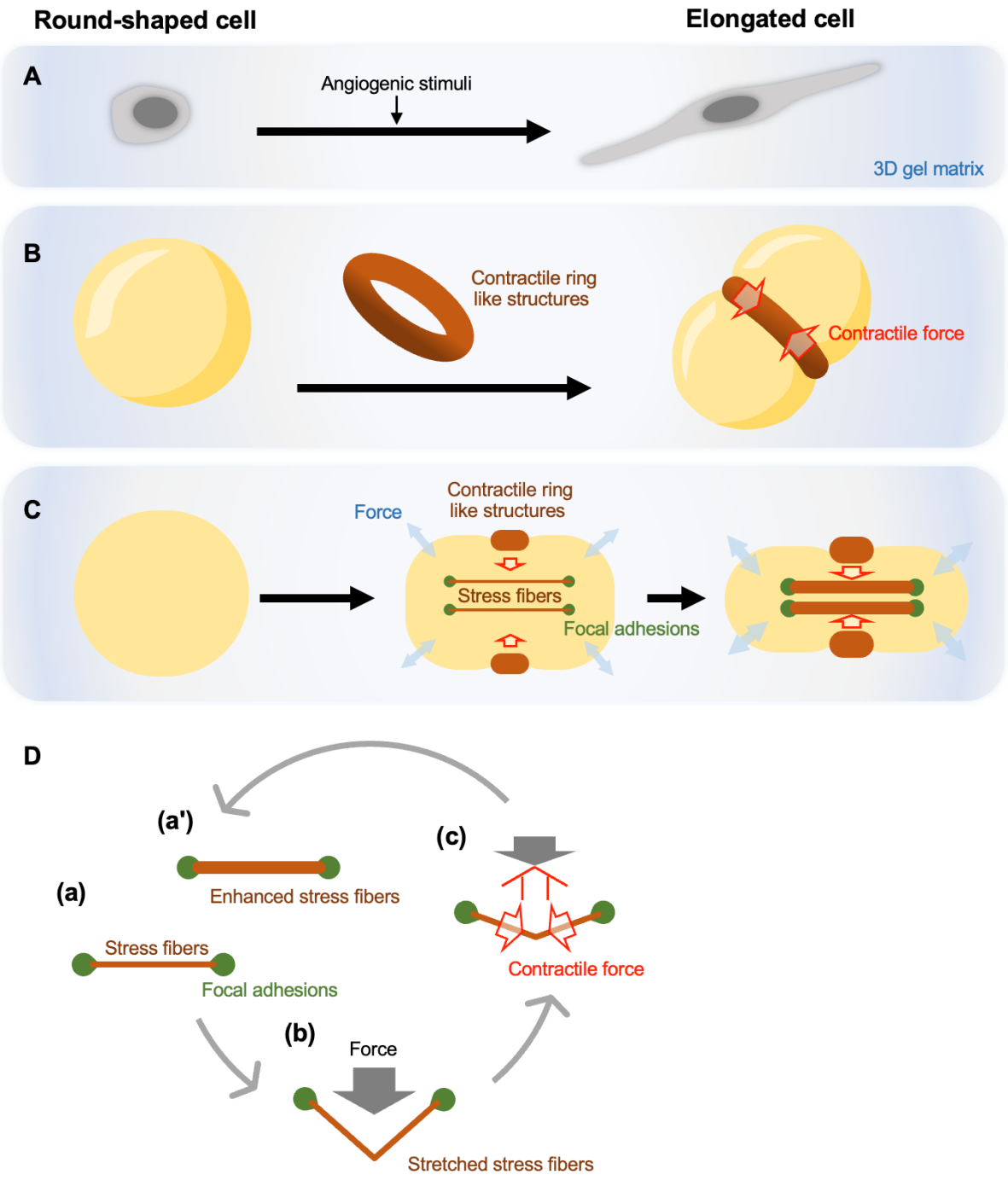

Supplementary Figure 1.

A hypothetical model of cell morphological change in three-dimensional gel matrix.

(A) Vascular endothelial cells are round in a 3D gel matrix and become elongated when activated by angiogenic stimuli such as VEGF-A. (B and C) Cytoplasm is represented as a sphere for easily understanding of the physical objects. (B) Actin and myosin system in cell cortex acts like a contractile ring (contractile ring like structure), gradually compressing the cytoplasm. The cells are deformed by the contractile force and become elongated. (C) Cross section image. Cell deformation by the contractile ring like structure is likely to generate action and reaction forces. These forces induce stress fibers, which parallel to the long cell axis, and contribute to the development and maintenance of the elongated cell shape. (D) A model of forces in stress fibers. Stress fibers are represented as elastic ropes for easily understanding of the physical property. (a) The ends of stress fiber are anchored at the extracellular matrix via the focal adhesions. (b) The stress fiber is stretched by a force. (c) Contractile forces are generated by the actin-myosin system, and the stress fiber wants to return to its original state. (a') Actin bundles are aligned, and the stress fiber is enhanced, probably depending on myosin activity. The resulting stress fibers may be key contributors to cell morphogenesis and maintenance.